Zurich Open Repository and Archive
University of Zurich
University Library
Strickhofstrasse 39
CH-8057 Zurich
www.zora.uzh.ch

Year: 2016

A peptidomimetic antibiotic targets outer membrane proteins and disrupts selectively the outer membrane in Escherichia coli

Urfer, Matthias ; Bogdanovic, Jasmina ; Lo Monte, Fabio ; Moehle, Kerstin ; Zerbe, Katja ; Omasits, Ulrich ; Ahrens, Christian H ; Pessi, Gabriella ; Eberl, Leo ; Robinson, John A

Abstract: Increasing antibacterial resistance presents a major challenge in antibiotic discovery. One attractive target in Gram-negative bacteria is the unique asymmetric outer membrane (OM), which acts as a permeability barrier that protects the cell from external stresses such as the presence of antibiotics. We describe a novel -hairpin macrocyclic peptide JB-95 with potent antimicrobial activity against E. coli. This peptide exhibits no cellular lytic activity, but electron microscopy and fluorescence studies reveal an ability to selectively disrupt the OM but not the inner membrane of E. coli. The selective targeting of the OM likely occurs through interactions of JB-95 with selected -barrel OM proteins including BamA and LptD as shown by photolabeling experiments. Membrane proteomic studies reveal rapid depletion of many -barrel OM proteins from JB-95-treated E. coli, consistent with induction of a membrane stress response and/or direct inhibition of the Bam folding machine. The results suggest that lethal disruption of the OM by JB-95 occurs through a novel mechanism of action at key interaction sites within clusters of -barrel proteins in the OM. These findings open new avenues for developing antibiotics that specifically target -barrel proteins and the integrity of the Gram-negative OM.

DOI: https://doi.org/10.1074/jbc.M115.691725

Posted at the Zurich Open Repository and Archive, University of Zurich
ZORA URL: https://doi.org/10.5167/uzh-120740
Journal Article
Accepted Version

Originally published at:
Urfer, Matthias; Bogdanovic, Jasmina; Lo Monte, Fabio; Moehle, Kerstin; Zerbe, Katja; Omasits, Ulrich; Ahrens, Christian H; Pessi, Gabriella; Eberl, Leo; Robinson, John A (2016). A peptidomimetic antibiotic targets outer membrane proteins and disrupts selectively the outer membrane in Escherichia coli. Journal of Biological Chemistry, 291:1921-1932.
DOI: https://doi.org/10.1074/jbc.M115.691725

JBC Papers in Press. Published on December 1, 2015 as Manuscript M115.691725
The latest version is at http://www.jbc.org/cgi/doi/10.1074/jbc.M115.691725

A Peptidomimetic Antibiotic Targets Outer Membrane Proteins and Disrupts Selectively the Outer Membrane in *Escherichia coli*

Matthias Urfer[1]*, Jasmina Bogdanovic[1]*, Fabio Lo Monte[1], Kerstin Moehle[1], Katja Zerbe[1], Ulrich Omasits[2], Christian H. Ahrens[3], Gabriella Pessi[4], Leo Eberl[4] and John A. Robinson[1]

[1] Department of Chemistry, University of Zurich, Winterthurerstrasse 190, 8057 Zurich,

[2] Institute of Molecular Systems Biology, ETH Zurich, Auguste-Piccard Hof 1, 8093 Zurich, Switzerland.

[3] Agroscope, Institute for Plant Production Sciences, Research Group Molecular Diagnostics, Genomics and Bioinformatics & Swiss Institute of Bioinformatics (SIB), Schloss 1, 8820 Wädenswil, Switzerland.

[4] Department of Microbiology, Institute of Plant Biology, University of Zurich, Zollikerstrasse 107, 8008 Zurich, Switzerland.

* contributed equally to the work described

Running title: Mechanism of action of a peptidomimetic antibiotic

To whom correspondence should be addressed: Professor John A. Robinson, Chemistry Department, University of Zurich, Winterthurerstrasse 190, 8057 Zurich, Switzerland. Telephone ++41 44 635 4242. E-mail: robinson@oci.uzh.ch

Keywords: Antibiotic action, peptides, outer membrane, Gram-negative bacteria, membrane protein.

Downloaded from http://www.jbc.org/ at UZH Hauptbibliothek / Zentralbibliothek Zuerich on February 8, 2016

Copyright 2015 by The American Society for Biochemistry and Molecular Biology, Inc.

Abstract

Increasing antibacterial resistance presents a major challenge in antibiotic discovery. One attractive target in Gram-negative bacteria is the unique asymmetric outer membrane (OM), which acts as a permeability barrier that protects the cell from external stresses such as the presence of antibiotics. We describe a novel ß-hairpin macrocyclic peptide JB-95 with potent antimicrobial activity against *E. coli*. This peptide exhibits no cellular lytic activity, but electron microscopy and fluorescence studies reveal an ability to selectively disrupt the OM but not the inner membrane of *E. coli*. The selective targeting of the OM likely occurs through interactions of JB-95 with selected ß-barrel OM proteins including BamA and LptD as shown by photolabeling experiments. Membrane proteomic studies reveal rapid depletion of many ß-barrel OM proteins from JB-95-treated *E. coli*, consistent with induction of a membrane stress response and/or direct inhibition of the Bam folding machine. The results suggest that lethal disruption of the OM by JB-95 occurs through a novel mechanism of action at key interaction sites within clusters of ß-barrel proteins in the OM. These findings open new avenues for developing antibiotics that specifically target ß-barrel proteins and the integrity of the Gram-negative OM.

Introduction

The discovery of novel antibiotics with new mechanisms of action is an important goal in antibiotic research to combat infections caused by multi-drug resistant bacteria, in particular, Gram-negative microorganisms with their unique asymmetric outer membrane (OM) (1). Naturally occurring cationic host defense peptides (HDPs) that form part of innate immunity in many organisms have recently attracted great interest in the search for new clinically useful antibiotics (2). We explore here an approach to antibiotic discovery based upon HDP-inspired macrocyclic peptidomimetics as a potential source of antibiotics displaying target selectivity and potency not seen with naturally occurring HDPs. In previous work, we described a family of macrocyclic ß-hairpin peptidomimetics with potent and selective antimicrobial activity against *Pseudomonas* spp. (3), which were shown to have a novel mechanism of action targeting the ß-barrel outer membrane protein LptD in *Pseudomonas aeruginosa* and inhibiting its key lipopolysaccharide (LPS) transport function in OM biogenesis (4). We report here the discovery of a new conformationally constrained ß-hairpin peptidomimetic (called JB-95) having potent antimicrobial activity against a panel of Gram-positive and Gram-negative bacteria, and in particular against *Escherichia coli*. JB-95 shows minimal inhibitory concentrations (MICs) of ≈ 0.25 μg/ml against *E. coli*, including many multi-drug resistant clinical strains. We report the solution structure of JB-95 and investigations into its mechanism of action against *E. coli*.

Experimental procedures

Peptide synthesis. The methods for synthesis and characterization of all peptides have been described previously (5). JB-95 was of >95% purity by analytical reverse phase HPLC *(Waters XBridge™* (C18, 50 x 19 mm, 5 μm, 135 Å) column with a gradient of 5-90% MeCN in H_2O (with 0.05% trifluoroacetic acid). ES-MS m/z 1970.1 ($[M+H]^+$, calc. 1970.0). See Supporting Information for full ^{1}H-NMR assignments. For the synthesis of the photoprobe PAL-95, Fmoc-Glu(biotiny-PEG)-OH (*Novabiochem*) and Fmoc-L-Photo-Pro-OH were used, along with other protected amino acids, following methods described earlier (3). PAL-95 purity was >95% by reverse phase HPLC (C18 Waters XBridge

Downloaded from http://www.jbc.org/ at UZH Hauptbibliothek / Zentralbibliothek Zuerich on February 8, 2016

column using a linear gradient of 10% to 60% MeCN in H_2O). ESI-MS m/z 593.6 $[M+4H]^{4+}$, 791.4 $[M+3H]^{3+}$. Full details for the synthesis of the fluorescent probe flJB-95 (MIC, 4 μg/ml) are given in the Supporting Information.

Antibacterial assays. Minimal inhibitory concentrations (MICs) were determined in microtitre plates, in Mueller-Hinton-I (MH-I) medium using the broth microdilution method (6). The kinetics of cell death was measured under the same conditions, by taking aliquots of medium and plating onto MH agar plates with growth overnight at 37ºC to determine CFUs.

NMR studies. The solution structure of JB-95 was determined by ^{1}H-NMR spectroscopy. Distance restraints were obtained from NOESY and ROESY spectra with a mixing time of 250 ms. The structure calculations were performed by restrained molecular dynamics in torsion angle space by applying the simulated annealing protocol implemented in the program DYANA (7). See Supporting Information for a full description of the results.

Macromolecular biosynthesis assays. Potential inhibitory effects of JB-95 on macromolecular synthesis (protein, RNA, DNA, cell wall) was monitored by incorporation of radioactively labeled precursors in chemically defined medium in a microplate format as described (8), using [^{3}H]-thymidine (80 Ci/mmol) and [^{3}H]-L-leucine (108 Ci/mmol), [^{3}H]-uridine (30 Ci/mmol) (from *Perkin Elmer*) and [^{3}H]-N-acetylglucosamine (30 Ci/mmol) and [^{3}H]-2,6-diaminopimelic acid (30 Ci/mmol) (from *Biotrend Chemikalien*).

Membrane permeabilization assay with SYTOX Green. *E. coli* ATCC25922 was grown in MH-I at 37°C with shaking to an OD_{600} of 0.2-0.3. The cells were collected and resuspended in MH-I to OD_{600} of 0.1. To this culture in a UV cuvette containing a small magnetic stirrer bar and 0.002% of Polyoxethylene80 (Tween80) was added SYTOX Green dye (0.5 µM) and the fluorescence signal was monitored for 400 s. The test antibiotic was added and the fluorescence intensity was recorded during 1 h (PerkinElmer LS55 spectrometer, excitation at 488 nm, emission at 525nm, and a slit width of 2.5 nm).

Fluorescence microscopy. *E. coli* ATCC25922 was grown in MH-II broth at 37ºC to an $OD_{600} \approx 0.5$-0.7. To an aliquot (200 μl) was added JB-95 or PMB and the culture was incubated at 30ºC for 1 h with shaking. Fluorescence dye (FM4-64 (1 μg/ml), SYTOX Green (0.5 μM), DAPI (2 μg/ml)) was added and the broth incubated at 0ºC for 10-15 min (DAPI & SYTOX Green) or 45-60 min (FM4-64). The cells were collected by centrifugation, washed with MH-II, then resuspended in MH-II (20 μl). The samples were imaged on a 1.1% agarose patch using a Leica CLSM SP8 gSTED 3X microscope, with laser excitation for DAPI (405 nm), SYTOX-Green (514 nm) or FM4-64 (520 nm) and a PMT or HyD detector. Alternatively, to an aliquot of cell suspension in MH-II was added the fluorescence probe flJB-95 (40 μg/ml). After 30 min at 30ºC the cells were washed twice with MH-II and examined as described above.

ß-Lactamase and ß-galactosidase assays. For periplasmic ß-lactamase expression, *E. coli* ATCC25922::pET3a was grown in MH-II broth to an OD_{600} of 0.3. The cells were collected, washed and resuspended in PBS supplemented with $CaCl_2$ (1mM) and $MgCl_2$ (0.5 mM) to an OD_{600} of 0.2. To this suspension in a UV cuvette with 0.02% BSA was added the chromogenic cephalosporin CENTA (100 μM). After 1 min the test antibiotic was added and the A_{405} was monitored over time. The dose-response with antibiotic was studied in a 24-well plate format using the cell suspension (848 μl), CENTA (100 µM), incubated at 37°C and shaken at 200 rpm for 1 h, before measuring

Downloaded from http://www.jbc.org/ at UZH Hauptbibliothek / Zentralbibliothek Zuerich on February 8, 2016

A_{405}. For cytoplasmic ß-galactosidase expression, *E. coli* XL1blue::pUC19 was grown in LB medium to an OD_{600} of 0.3. LacZα expression was induced with IPTG (100 μg/ml) and incubation continued at 37ºC for 1 h to an OD_{600} ≈ 0.6. The cells were collected, washed twice with fresh LB medium, and then resuspended in PBS supplemented with $CaCl_2$ (1mM) and $MgCl_2$ (0.5 mM) to an OD_{600} of 0.3. The cell suspension was distributed into a 24-well plate with antibiotic, substrate (O-nitrophenyl-ß-D-galactoside) was added (0.5 mM) and incubated at 37ºC with shaking for 1 h. The cells were then removed by centrifugation and the A_{420} was measured.

Electron microscopy (EM). EM studies with *E. coli* ATCC25922 treated with JB-95 were performed using methods described earlier (3).

Proteomics. *E. coli* ATCC25922 was grown in LB to end-exponential phase with JB-95 (5 μg/ml) causing ≈50% growth inhibition. Cells from treated and untreated cultures were harvested by centrifugation (three biological replicates each), lysed by French press and membranes were isolated by differential centrifugation (30 min at 3005 g followed by 45 min at 100'000 g). The membrane protein pellet was resuspended in PBS and ≈ 10 μg of protein from treated and untreated cells was analyzed by 12% SDS-PAGE with Coomassie staining (Figure 6A).

Proteins extracted from total membrane fractions of *E. coli* grown in LB medium with or without JB-95 were first separated by 12% SDS_PAGE. After reduction and carbamidomethylation, the proteins were digested with trypsin (*Promega*, Madison, WI, USA), and the resulting peptides were separated by RP-HPLC and analyzed by a LTQ-Orbitrap Velos mass spectrometer (*Thermo Fisher Scientific*, Waltham, MA, USA) interfaced with a nanoelectrospray source. Mass spectra were further processed with an in-house processing pipeline (9) that extracts fragment ion mass spectra from Thermo RAW files using msconvert (ProteoWizard, version 3.0.3831) and searches for matching peptides in an *E. coli* K12 protein database (substrain MG1655, NC_000913.3) containing 256 common contaminants (e.g. human keratin, trypsin) with the search engine MS-GF+ (v9979), here using a 20 ppm mass tolerance window. Using the decoy option of MS-GF+, the list of peptide spectrum matches (PSMs) was filtered to an estimated overall false discovery rate (FDR) of 0.1%, which amounted to a protein level FDR of about 1% when requiring two unambiguous peptides (class 1a or 3a based on a PeptideClassifier analysis (10) or three spectra for protein identification in either condition). A total of 1740 proteins were identified overall. DESeq2 (11) (version 1.4.5) was used to identify the most significantly regulated proteins, here applying a q-value threshold of 0.06 (Benjamini-Hochberg adjusted p-value indicating that roughly 3 false positives are expected among the top 56 differentially regulated proteins). Proteomics data associated with this manuscript can be downloaded from the ProteomeXchange under accession number PXD002588.

Functional analysis. For prediction of ß-barrel OM proteins, and subcellular localization we relied on the publicly available BOMP (12) and PSORTb v3.0 (13) web servers (Table 2), as described (14).

qPCR analysis. *E. coli* ATCC25922 cells were grown to end-exponential phase in the presence or absence of JB-95. Cell harvest, RNA extraction and cDNA synthesis were as previously described (15). The expression of *E. coli* ATCC25922 genes *wcaI* (EG11790), *wzc* (EG13568), *murC* (EG10619), *arnA* (EG14091), *ompF* (EG10671), *lptD* (EG11569), *lamB* (EG10528), and *bamA* (EG12676) was analyzed by qRT-PCR using Brilliant III Ultra-Fast SYBR® Green QPCR Master Mix (*Agilent*, Switzerland) and a

Downloaded from http://www.jbc.org/ at UZH Hauptbibliothek / Zentralbibliothek Zuerich on February 8, 2016

Mx3000P instrument (Agilent, Switzerland). Each PCR reaction was run in triplicate with 3 dilutions of cDNA (15, 7.5 and 3.75 ng) using 15 μl 2x Brilliant III Ultra-Fast SYBR® Green QPCR Master Mix and 5 μM of individual primers in a total volume of 24 μl. Melting curves were generated for verifying the specificity of the amplification. The primers used are listed in the Supporting Information.

Photolabeling experiments. Photolabeling experiments with *E. coli* K12 MG1655 and *E. coli* ATCC25922, and the probe PAL-95 (Figure 1A) were performed using methods described in detail elsewhere (3).

Results

Antimicrobial activity. A screening effort uncovered the backbone macrocyclic tetradecapeptide, called JB-95 (*cyclo*-(Trp[1]-Arg[2]-Ile[3]-Arg[4]-Ile[5]-^{D}Arg[6]-Trp[7]-Lys[8]-Arg[9]-Leu[10]-Arg[11]-Arg[12]-^{D}Pro[13]-Pro[14]) see Figure 1A). JB-95 has good antimicrobial activity against a panel of Gram-negative and Gram-positive bacteria (Table 1). However, the antimicrobial activity was considerably higher against *E. coli* (MIC $\approx$ 0.25 μg/ml) and was maintained across a panel of *E. coli* clinical strains showing resistance to a variety of known antibiotics. The enantiomer of JB-95 (ent-JB-95) shows 2-4 fold reduced antimicrobial activity against all tested organisms. The kinetics of *E. coli* ATCC25922 cell killing in a microplate format revealed a bactericidal action over several hours at 2-8xMIC, but not the rapid killing caused by the cell lytic peptide protegrin I (PG-I) (Figure 1B).

Structural NMR studies. The average solution structure of JB-95 was determined by ^{1}H-NMR spectroscopy in aqueous buffer. A detailed analysis of 2D-^{1}H NOESY and ROESY spectra revealed a dense network of cross-strand nuclear Overhauser effects (NOEs), which along with other data, including amide chemical shift dispersions, $^{3}J_{HNH\alpha}$ coupling constants, amide H/D exchange rates and temperature coefficients (see Supporting Information), clearly indicate a stable conformationally arrested ß-hairpin structure within the JB-95 macrocycle. Structure calculations were performed by restrained molecular dynamics in torsion angle space with the program DYANA (7). A bundle of 20 conformations incurring the lowest DYANA target function were selected, and a single representative structure is shown in Figure 2. All structures contain type-II' ß-turns within the template (D-Pro[13]-L-Pro[14]) and at the tip of the loop (D-Arg[6]-L-Lys[7]), with regular ß-strands connecting the two turn structures (16). The NMR studies show that JB-95 adopts a stable ß-hairpin conformation in aqueous solution.

Permeabilization of the OM. JB-95 showed no significant lytic activity on human red blood cells at a concentration of 100 μg/ml, which is well above the MIC. The permeabilizing effect of JB-95 on *E. coli* ATCC25922 was investigated using the fluorescent dye SYTOX Green. *E. coli* cells grown in MH-I broth and then treated with SYTOX Green and JB-95 showed no rapid increase in fluorescence over 1 h (Figure 1C), whereas, treatment of cells with polymyxin B (PMB) leads within 20 min to a rapid characteristic increase in green fluorescence, as both IM and OM are permeabilized and the dye gains access to and binds nucleic acids in the cytoplasm.

Macromolecular synthesis assays. We investigated the influence of JB-95 on macromolecule biosynthesis in *E. coli* ATCC25922 by monitoring the incorporation of radioactively labeled precursors in chemically defined medium in a microplate format (8). Labeling starts with exponentially growing cultures at an OD_{600} of 0.3, and the incorporation of label is performed over a fixed period of only 20 min to reveal direct effects of the antibiotic, before secondary

Downloaded from http://www.jbc.org/ at UZH Hauptbibliothek / Zentralbibliothek Zuerich on February 8, 2016

effects and cell death become prominent. No significant inhibition by JB-95 was observed of protein, RNA or DNA biosynthesis, whereas control experiments with known antibiotics gave rise to the anticipated inhibitory effects (not shown). Interestingly, JB-95 reproducibly caused a significant stimulation of radioactivity incorporated from [^{3}H]-N-acetylglucosamine into macromolecules (Figure 1D). In contrast, only a minor stimulation of tritium incorporation was observed in labeling experiments using [^{3}H]-diaminopimelic acid. The results are not consistent with a direct inhibition of cell wall/membrane biosynthesis.

Microscopy studies. The effects of JB-95 on *E. coli* cells grown in MH with concentrations of JB-95 causing 50% growth inhibition for 1 h at 30°C were analyzed using a high-resolution stimulated emission depletion (STED) fluorescence microscope, with staining of membranes by the membrane dye FM4-64, of nucleoids by 4',6-diamidino-2-phenylindole (DAPI), and using SYTOX Green to detect permeabilized cells (Figure 3). The stained nucleoids were not influenced significantly by JB-95, and apart from a small number of dead cells, no significant staining (<10% of cells) was observed by SYTOX Green. Relative to untreated cells, however, a large proportion (>50%) of cells treated with JB-95 were elongated, and contained unusual accumulations of membrane-like material stained by FM4-64 (Figure 3).

A derivative of JB-95 labeled with Alexafluor-488 (called flJB-95, see Figure 1A) was prepared to study the uptake of the antibiotic by fluorescence microscopy. This derivative shows an MIC of ≈4 μg/ml, and so retains a good antimicrobial activity against *E. coli*. Cells were shaken with flJB-95 for 30 min in MH broth and then examined using STED microscopy. The staining pattern (Figure 3I) revealed that the probe was concentrated into clusters or islands, consistent with localized binding sites on the cell surface.

Evidence for a perturbation in membrane morphology was revealed by transmission electron microscopy (TEM) of cells grown in LB with JB-95 at concentrations causing ≈50% inhibition of growth. In comparison to untreated controls, sections of treated *E. coli* cells appeared with a minimal periplasmic space, and showed distinct ruptures in the OM, without any apparent disturbance to the IM (Figure 4B-C). Many cells also showed accumulations of unusual membrane-like material between the IM and the OM (Figure 4D). These microscopy studies indicate a dramatic effect of JB-95 on the outer cell membrane. When JB-95-treated cells were examined by scanning EM (SEM), the most notable feature compared to controls was the appearance of knob-like structures over the surface of most cells, which was not seen in the control (Figure 4E-F).

Susceptibility to detergents and antibiotics. *E. coli* cells grown with JB-95 at concentrations causing ≈50% growth inhibition were plated onto agar containing 0.5% SDS and 0.5 mM EDTA, or a selection of other antibiotics. The results revealed a dramatic increase (ca. 10^4 fold) in the sensitivity of JB-95-treated cells to growth on agar containing SDS/EDTA, compared to untreated cells, consistent with a compromised OM permeability barrier allowing exposure of the IM to the lethal actions of detergent (Figure 5A). In agar disk diffusion assays the treated cells also showed enhanced sensitivity to gentamycin, chloramphenicol, nalidixic acid and tetracycline.

ß-Lactamase and ß-galactosidase assays. *E. coli* expressing high levels of periplasmic ß-lactamase was grown in MH broth to an OD_{600} of 0.3. Cells were then collected and treated with JB-95. Cell-free ß-lactamase activity was

Downloaded from http://www.jbc.org/ at UZH Hauptbibliothek / Zentralbibliothek Zuerich on February 8, 2016

detected using the chromophoric cephalosporin substrate CENTA as a function of time and drug concentration, which revealed a rapid release of the enzyme (Figure 5B/C). A similar release was also observed from cells treated with PMB, which is known to permeabilize both the OM and IM of *E. coli*, but (as expected) not from cells exposed to ciprofloxacin. We also examined the effect of JB-95 on *E. coli* expressing cytoplasmic ß-galactosidase. These assays showed that JB-95-treated cells do not release ß-galactosidase into the medium, whereas release is observed when cells are treated with PMB or PG-I, consistent with the known effects of PG-I and PMB on the permeability of both the IM and OM (Figure 5D).

Effects on the OM proteome. The influence on the OM proteome of *E. coli* ATCC25922 grown with JB-95 concentrations causing ≈50% growth inhibition was investigated. Whole membrane fractions isolated by differential centrifugation from both treated and non-treated control cells were analyzed by SDS-PAGE. The gels reveal a dramatic decrease in the relative amounts of some membrane proteins compared to the untreated control (Figure 6A). To identify membrane proteins differentially expressed in the presence of JB-95, a semi-quantitative proteomic analysis was performed using in-gel digestion and ESI-LC-MS/MS-analyses. Data analysis was performed using DESeq2 to identify the most significantly regulated proteins between treated and untreated cells (each measured in triplicate) (11,14). The protein expression profiling experiment identified a total of 1740 proteins. Applying a stringent selection of differentially expressed proteins ($q \leq 0.06$) we identified 19 significantly up-regulated and 37 down-regulated proteins (Figure 6B) in JB-95 treated cells, as recorded in Table 2. We observed that ß-barrel OM proteins and the larger group of PSORTb OM proteins are significantly enriched among differentially regulated proteins (P-value < 10^{-15}, respectively). Most notable amongst the up-regulated are proteins involved in capsule biosynthesis and export (Wzc, Wza, Gmd), lipid A modifications (ArnA, ArnC, EptA), proteins involved in OM stress responses (ClpX, DegP, PhoQ, RstB) and drug efflux (AcrD). Equally notable amongst the significantly down-regulated proteins is the large number of OM ß-barrel proteins, porins and transporters (Table 2). The level of the ß-barrel folding protein BamA was not significantly changed by JB-95. However, suppressive effects on BamA might be compensated by up-regulation as part of an envelope stress response (σ^E). To independently assess the proteomics results, quantitative real-time PCR (qRT-PCR) analysis was performed on independent biological replicate cultures, targeting selectively genes involved in capsule and murein biosynthesis (*wcaI*, *wzc* and *murC*), a UDP-L-Ara4n-formyl transferase encoded by *arnA*, as well as *ompF*, *lptD*, *lamB* and *bamA*. These results revealed genes that are strongly up-regulated (*wcaI* (+10 fold), *wzc* (+6 fold), *arnA* (+3 fold)) others down-regulated (*ompF* (-23 fold), *lamB* (-5 fold)) and some whose levels are not significantly changed by JB-95 (*lptD* (-1.3 fold), *bamA* (+1.3 fold), *murC* (+1.6 fold)). A good correlation is seen between the results at the mRNA and protein levels for many of these genes (Table 2), including *bamA,* whose level is not significantly affected by JB-95.

Photolabeling experiments. Photolabeling experiments were carried out with the photoprobe PAL-95, which is identical to JB-95 except for the replacement of L-Pro[14] by the photoreactive diazirine-containing L-photoproline (3), and of L-Arg[9] by a Glu(PEG_2-biotin) (residue Z in Figure 1A). PAL-95 retained a high antimicrobial activity against *E. coli* (Table 1). Experiments were performed with both the clinical isolate

Downloaded from http://www.jbc.org/ at UZH Hauptbibliothek / Zentralbibliothek Zuerich on February 8, 2016

(ATCC25922) and a genetically well-characterized K12 strain. Results of photolabeling experiments in *E. coli* K12 MG1655 are shown in Figure 7. After photolabeling cells with PAL-95 the OM proteome was extracted and analyzed by 2D gel electrophoresis. Photolabeled, biotinylated proteins were detected after blotting to a membrane by chemiluminescence. Comparison of the blots with Coomassie stained 2D gels from unlabeled OM proteome allowed identification of photolabeled BamA and LptD on the basis of their unique and characteristic positions in the 2D gel, including characteristic changes in the mobility of LptD in the gel before and after reduction by DTT, as described earlier (18). Other photolabeled proteins were detected around 67kDa and 40 kDa at positions expected for BtuB, and LamB and FadL, respectively. The most abundant OM proteins (OmpA/F) are not labeled by the photoprobe. Photolabeling experiments with PAL-95 and *E. coli* ATCC25922 gave similar results, and also showed labeling of BamA, LptD, LamB and FadL, but not BtuB (not shown). These results show that JB-95 interacts with several ß-barrel proteins in the OM of *E. coli,* including in both strains the essential proteins LptD and BamA required for the biogenesis of the OM.

Discussion

The macrocyclic ß-hairpin-shaped peptide JB-95 displays antimicrobial activity against Gram-negative bacteria and *S. aureus* (Table-1). However, the activity against *E. coli* is an order of magnitude higher, suggesting a selective mechanism of action that merited further investigation. JB-95 shows no cellular membranolytic activity, and the kinetics of bacterial cell death reveals a clear difference between the actions of PG-I and JB-95 (Figure 1B). PG-I kills a wide spectrum of Gram-positive and Gram-negative bacteria within 20-30 min of cell contact at micromolar concentrations through a lytic mechanism of action (19). Furthermore, exposing cells to JB-95 does not lead to rapid cytoplasmic uptake of SYTOX Green, in contrast to cytoplasmic staining seen after treatment with PG-I or PMB (Figure 1C and 3).

TEM studies provide evidence that JB-95-treated *E. coli* suffer multiple ≈ 50 nm breaches of the OM (Figure 4) without visible effects on the IM. This differential effect on IM and OM merits further attention and discussion. Firstly, amphiphilic cationic antimicrobial peptides (CAMPs) with a membranolytic mode of action, such as PG-I and PGLa, rapidly destabilize both inner and outer membranes of *E. coli* at concentrations close to the MIC (19-21). Permeabilization of both the OM and IM of *E. coli* by the human antimicrobial peptide LL-37, with uptake into the cytoplasm of SYTOX Green, has been documented by real-time fluorescence microscopy (22). Indeed, many CAMPs, including examples isolated from the innate immune systems of various organisms as well as others of purely synthetic origin, physically impair membrane bilayers (23-25). Several models have been described to explain such activity, including formation of pore-like structures and micellization of the membrane bilayer (26-28), although there is increasing evidence that some CAMPs have alternative mechanisms of action, not directly related to damage of the cytoplasmic membrane (29-32).

The antibiotic PMB permeabilizes the OM before targeting and disrupting the cytoplasmic membrane in *E. coli* (33,34). As a result, PMB causes release into the medium of not only periplasmic ß-lactamase but also of cytoplasmic ß-galactosidase (35,36), as confirmed in our studies (Figure 5). Earlier electrical measurements with reconstituted planar bilayers suggested an initial electrostatic interaction of PMB with the LPS outer leaflet, followed by formation of

Downloaded from http://www.jbc.org/ at UZH Hauptbibliothek / Zentralbibliothek Zuerich on February 8, 2016

transient membrane lesions of about 3 nm diameter (37,38). The lesions allow PMB and other small molecules and ions to permeate the OM in both directions (self-promoted uptake) (39), but appear to be quite different in size and nature to the lesions induced by JB-95 (Figure 4). Although we observe complete release into the medium of periplasmic ß-lactamase after treatment of cells with JB-95, almost no release occurs of ß-galactosidase from the cytoplasm, in contrast to observations made with PMB (Figure 5). Moreover, the damage to the OM caused by JB-95 accounts for the greatly enhanced sensitivity of JB-95-treated cells to SDS/EDTA on agar (Figure 5A).

The integrity of the OM in Gram-negative bacteria is essential for survival and is monitored by several transcriptional signaling systems, which can initiate damage-repair responses. One of these is the σ^E stress-response, which is activated by a dual-signal comprising incorrectly folded OM proteins and by off-pathway intermediates in LPS transport and assembly in the periplasm (40,41). In response to these signals, σ^E *stimulates* the transcription of many genes, including all the machinery required for the transport and assembly of LPS and OM proteins into the OM (42-44). However, σ^E also induces expression of small regulatory RNAs, MicA and RydB, which act to *inhibit* synthesis of several ß-barrel OM proteins (45,46). The Rcs phosphorelay is another signaling system in Gram-negative bacteria, which is induced by OM and cell wall damage, and controls the expression of genes involved in motility, extracellular polysaccharide and biofilm formation, virulence and periplasmic quality control (47). Rcs regulates production of capsular polysaccharide (colanic acid) and extracellular polysaccharide, which help stabilize the OM and combat envelope stress (48). Lastly, the PhoPQ two-component regulatory system in Gram-negative bacteria is important for bacterial survival in host tissues, and senses CAMPs and induces responses that regulate the protein and lipid content of the IM and OM (49,50). In particular, PhoPQ induced modifications occur to the lipid A segment of LPS before transport to the cell surface, such as addition of cationic moieties including 4-amino-4-deoxyarabinose (4-AraN), that reduce the net negative charge of the LPS and contribute to bacterial resistance to CAMPs and PMB (51).

This background is helpful in understanding the response of *E. coli* to JB-95. Thus the stimulated incorporation of radiolabeled N-acetylglucosamine into macromolecules (Figure 1D) is likely due to a stimulation of capsular polysaccharide production. The appearance in scanning EM pictures of knob-like structures over the surface of cells treated with JB-95 (Figure 4F) are reminiscent of previously reported surface exposed poly-GlcNAc (52). The dimensions of the knobs appears quite different from the surface blebs that have been observed upon inhibition of σ^E in *E. coli* (53), or the membrane protusions typical of PMB-treated cells (54,55). Moreover, the results of proteomic and qRT-PCR studies show up-regulation triggered by JB-95 of key proteins involved in capsular polysaccharide biosynthesis and excretion (Wza, Wzc, Wcal) (Table 2). The unusual accumulations of membrane-like material observed by fluorescence and TEM (Figure 3D and 4D) might be explained by a build-up of intermediates in capsular polysaccharide or LPS biosynthesis, linked to a C_{55}-undecaprenoid lipid carrier (44,56). The lipid-bilayer accumulations appear approximately three times thicker than a membrane phospholipid bilayer (compare OM, Figure 4D, arrows). Moreover, since down-regulation of LptD was observed here in the proteomic studies, impaired LPS transport to the cell surface should be expected, which typically leads to dramatic membrane ultrastructural

Downloaded from http://www.jbc.org/ at UZH Hauptbibliothek / Zentralbibliothek Zuerich on February 8, 2016

changes (57-59). Mutations in the inner membrane LPS and phospholipid flippase MsbA have also been shown to cause inner membrane reduplications and invaginations due to inhibition of lipid export (60).

The proteomic studies reveal that many ß-barrel OM proteins are down-regulated in JB-95-treated cells (Figure 6 and Table 2). These results can be at least partly explained by a σ^E-dependent response acting through the small regulatory RNAs MicA and/or RydB, which have been shown to inhibit the synthesis of many ß-barrel OM proteins in *E. coli* (45,46) (Table 2). Interestingly, the essential OM LPS translocase LptD was significantly depleted in the proteomics study (Table 2), although by qRT-PCR only a minor change was seen. In contrast, the regulation of the essential ß-barrel folding machine BamA was largely unaffected by JB-95 in both the proteomic and qRT-PCR assays. Since BamA is known to be essential for the correct folding and insertion of most ß-barrel proteins into the OM, including LptD (42), an alternative explanation for the depletion of many ß-barrel OM proteins may be that JB-95 inhibits the function of BamA. The OM protein Wza, which is upregulated by JB-95 (Table 2), has a transmembrane domain of eight α-helices (61) that is not dependent on BamA for insertion into the OM (62). Other significant JB-95-induced proteomic changes are increased levels of proteins active in maintenance of the periplasm (DegP, ClpX) (63) and modifications to lipid A through the PhoP/Q response (PhoQ, ArnA, ArnC, EptA) (51).

High-resolution fluorescence microscopy of *E. coli* cells exposed to the fluorescently labeled form of JB-95 (flJB-95) shows the peptide concentrated in a punctated pattern (Figure 3H) in the OM, rather than binding uniformly over the cell surface. Early EM and recent fluorescence labeling studies have shown that many OM proteins in *E. coli* associate into islands or patches in the OM (64-67). The labeling patterns seen with flJB-95 suggest that the peptide is associating with OM protein patches. This conclusion is supported by the photolabeling studies, which show that JB-95 interacts with several ß-barrel OM proteins (Figure 7), interactions that might mediate the disruptive effects on the OM. For example, membrane thinning caused by contact of lipid groups with membrane-bound ß-barrel proteins might provide sensitive sites where OM disruption mediated by JB-95 could occur (68). Alternatively, some of the photolabeled ß-barrel OM proteins, including BamA and LptD in two different *E. coli* strains, expose ß-strands by transient opening of the ß-barrel to form lateral gates during transport, folding or translocation of substrate molecules across the membrane (69-75), and might be vulnerable to interactions with peptidomimetics having folded ß-hairpin structures. These proposals might be testable in future work using reconstituted ß-barrel proteins *in vitro*. Finally, optimization of both the antimicrobial and drug-like properties of molecules like JB-95 could have important implications for the development of a new class of antibiotics specifically targeting the Gram-negative OM.

Downloaded from http://www.jbc.org/ at UZH Hauptbibliothek / Zentralbibliothek Zuerich on February 8, 2016

Acknowledgements

The authors thank the Swiss National Science Foundation for financial support; Dr. Urs Ziegler and Dr. Andres Käch, Center for Microscopy and Image Analysis, University of Zürich, for electron and fluorescence microscopy studies; Dr. Peter Hunziker, Functional Genomics Center Zurich for proteomics support; Michael Schmid (Agroscope) for proteomics analyses; Dr.

Krystyna Patora-Komisarska for help with synthesis; and Annelies Meier, Isabell Scholl, Alexander Grunau and Dr. Yilei Liu for technical support.

Conflict of interest

The authors declare that they have no conflicts of interest with the contents of this article.

Author contributions

JAR and LE conceived the study and oversaw all experimental work. JB and MU synthesized peptides. JB, MU, FLM and KZ performed microbiological, microscopy, photolabeling and fluorescence studies. UO, CHA and GP assisted with proteomics studies; KM performed structural studies by NMR. All authors reviewed the results and approved the final version of the manuscript.

References

1. Page, M. G. P., and Bush, K. (2014) Discovery and development of new antibacterial agents targeting Gram-negative bacteria in the era of pandrug resistance: is the future promising? *Curr. Opin. Pharmacol.* **18**, 91-97
2. Galdiero, S., Falanga, A., Berisio, R., Grieco, P., Morelli, G., and Galdiero, M. (2015) Antimicrobial Peptides as an Opportunity Against Bacterial Diseases. *Curr. Med. Chem.* **22**, 1665-1677
3. Srinivas, N., Jetter, P., Ueberbacher, B. J., Werneburg, M., Zerbe, K., Steinmann, J., Van der Meijden, B., Bernardini, F., Lederer, A., Dias, R. L. A., Misson, P. E., Henze, H., Zumbrunn, J., Gombert, F. O., Obrecht, D., Hunziker, P., Schauer, S., Ziegler, U., Kach, A., Eberl, L., Riedel, K., DeMarco, S. J., and Robinson, J. A. (2010) Peptidomimetic Antibiotics Target Outer-Membrane Biogenesis in Pseudomonas aeruginosa. *Science* **327**, 1010-1013
4. Werneburg, M., Zerbe, K., Juhas, M., Bigler, L., Stalder, U., Kaech, A., Ziegler, U., Obrecht, D., Eberl, L., and Robinson, J. A. (2012) Inhibition of Lipopolysaccharide Transport to the Outer Membrane in Pseudomonas aeruginosa by Peptidomimetic Antibiotics. *Chembiochem* **13**, 1767-1775
5. Jiang, L., Moehle, K., Dhanapal, B., Obrecht, D., and Robinson, J. A. (2000) Combinatorial biomimetic chemistry: Parallel synthesis of a small library of ß-hairpin mimetics based on loop III from human platelet-derived growth factor B. *Helv. Chim. Acta* **83**, 3097-3112
6. Andrews, J. M. (2001) Determination of minimum inhibitory concentrations. *J. Antimicrob. Chemother.* **48**, 5-16
7. Güntert, P., Mumenthaler, C., and Wüthrich, K. (1997) Torsion angle dynamics for NMR structure calculation with the new program Dyana. *J. Mol. Biol.* **273**, 283-298

Downloaded from http://www.jbc.org/ at UZH Hauptbibliothek / Zentralbibliothek Zuerich on February 8, 2016

8. Cunningham, M. L., Kwan, B. P., Nelson, K. J., Bensen, D. C., and Shaw, K. J. (2013) Distinguishing On-Target versus Off-Target Activity in Early Antibacterial Drug Discovery Using a Macromolecular Synthesis Assay. *J. Biomol. Screen.* **18**, 1018-1026
9. Omasits, U., Quebatte, M., Stekhoven, D. J., Fortes, C., Roschitzki, B., Robinson, M. D., Dehio, C., and Ahrens, C. H. (2013) Directed shotgun proteomics guided by saturated RNA-seq identifies a complete expressed prokaryotic proteome. *Genome Res.* **23**, 1916-1927
10. Qeli, E., and Ahrens, C. H. (2010) PeptideClassifier for protein inference and targeted quantitative proteomics. *Nat. Biotech.* **28**, 647-650
11. Love, M. I., Huber, W., and Anders, S. (2014) Moderated estimation of fold change and dispersion for RNA-seq data with DESeq2. *Genome Biol.* **15**, 550
12. Berven, F. S., Flikka, K., Jensen, H. B., and Eidhammer, I. (2004) BOMP: a program to predict integral β-barrel outer membrane proteins encoded within genomes of Gram-negative bacteria. *Nucl. Acids Res.* **32**, W394-W399
13. Yu, N. Y., Wagner, J. R., Laird, M. R., Melli, G., Rey, S., Lo, R., Dao, P., Sahinalp, S. C., Ester, M., Foster, L. J., and Brinkman, F. S. L. (2010) PSORTb 3.0: improved protein subcellular localization prediction with refined localization subcategories and predictive capabilities for all prokaryotes. *Bioinformatics* **26**, 1608-1615
14. Stekhoven, D. J., Omasits, U., Quebatte, M., Dehio, C., and Ahrens, C. H. (2014) Proteome-wide identification of predominant subcellular protein localizations in a bacterial model organism. *J. Proteomics* **99**, 123-137
15. Pessi, G., Braunwalder, R., Grunau, A., Omasits, U., Ahrens, C. H., and Eberl, L. (2013) Response of Burkholderia cenocepacia H111 to Micro-Oxia. *PLoS ONE* **8**, e72939
16. Robinson, J. A. (2008) ß-Hairpin peptidomimetics: design, structures and biological activities. *Accts. Chem. Res.* **41**, 1278-1288
17. Bebrone, C., Moali, C., Mahy, F., Rival, S., Docquier, J. D., Rossolini, G. M., Fastrez, J., Pratt, R. F., Frère, J.-M., and Galleni, M. (2001) CENTA as a Chromogenic Substrate for Studying β-Lactamases. *Antimicrob. Agents Chemother.* **45**, 1868-1871
18. Ruiz, N., Chng, S. S., Hiniker, A., Kahne, D., and Silhavy, T. J. (2010) Nonconsecutive disulfide bond formation in an essential integral outer membrane protein. *Proc. Natl. Acad. Sci. USA* **107**, 12245-12250
19. Steinberg, D. A., Hurst, M. A., Fujii, C. A., Kung, A. H., Ho, J. F., Cheng, F. C., Loury, D. J., and Fiddes, J. C. (1997) Protegrin-1: a broad-spectrum, rapidly microbicidal peptide with in vivo activity. *Antimicrob. Agents Chemother.* **41**, 1738-1742
20. da Silva Jr, A., and Teschke, O. (2003) Effects of the antimicrobial peptide PGLa on live Escherichia coli. *Biochim. Biophys. Acta Mol. Cell Res.* **1643**, 95-103
21. Hartmann, M., Berditsch, M., Hawecker, J., Ardakani, M. F., Gerthsen, D., and Ulrich, A. S. (2010) Damage of the Bacterial Cell Envelope by Antimicrobial Peptides Gramicidin S and PGLa as Revealed by Transmission and Scanning Electron Microscopy. *Antimicrob. Agents Chemother.* **54**, 3132-3142
22. Sochacki, K. A., Barns, K. J., Bucki, R., and Weisshaar, J. C. (2011) Real-time attack on single Escherichia coli cells by the human antimicrobial peptide LL-37. *Proc. Natl. Acad. Sci. USA* **108**, E77-E81
23. Hancock, R. E. W., and Diamond, G. (2000) The role of cationic antimicrobial peptides in innate host defences. *Trends Microbiol.* **8**, 402-410

Downloaded from http://www.jbc.org/ at UZH Hauptbibliothek / Zentralbibliothek Zuerich on February 8, 2016

24. Zasloff, M. (2002) Antimicrobial peptides of multicellular organisms. *Nature* **415**, 389-395
25. Fjell, C. D., Hiss, J. A., Hancock, R. E. W., and Schneider, G. (2012) Designing antimicrobial peptides: form follows function. *Nat. Rev. Drug Discov.* **11**, 37-51
26. Matsuzaki, K., Yoneyama, S., and Miyajima, K. (1997) Pore formation and translocation of melittin. *Biophys. J.* **73**, 831-838
27. Shai, Y. (2002) Mode of action of membrane active antimicrobial peptides. *Pept. Sci.* **66**, 236-248
28. Brogden, K. A. (2005) Antimicrobial peptides: pore formers or metabolic inhibitors in bacteria? *Nat. Rev. Micro.* **3**, 238-250
29. Wu, M., Maier, E., Benz, R., and Hancock, R. E. W. (1999) Mechanism of Interaction of Different Classes of Cationic Antimicrobial Peptides with Planar Bilayers and with the Cytoplasmic Membrane of Escherichia coli. *Biochemistry* **38**, 7235-7242
30. Peschel, A., and Sahl, H.-G. (2006) The co-evolution of host cationic antimicrobial peptides and microbial resistance. *Nat Rev. Microbiol.* **4**, 529-536
31. Roy, R. N., Lomakin, I. B., Gagnon, M. G., and Steitz, T. A. (2015) The mechanism of inhibition of protein synthesis by the proline-rich peptide oncocin. *Nat. Struct. Mol. Biol.* **22**, 466-469
32. Seefeldt, A. C., Nguyen, F., Antunes, S., Perebaskine, N., Graf, M., Arenz, S., Inampudi, K. K., Douat, C., Guichard, G., Wilson, D. N., and Innis, C. A. (2015) The proline-rich antimicrobial peptide Onc112 inhibits translation by blocking and destabilizing the initiation complex. *Nat. Struct. Mol. Biol.* **22**, 470-U459
33. Yu, Z. L., Qin, W. R., Lin, J. X., Fang, S. S., and Qiu, J. P. (2015) Antibacterial Mechanisms of Polymyxin and Bacterial Resistance. *Biomed Res. Int.*, 11
34. Velkov, T., Thompson, P. E., Nation, R. L., and Li, J. (2010) Structure–Activity Relationships of Polymyxin Antibiotics. *J. Med. Chem.* **53**, 1898-1916
35. Dixon, R. A., and Chopra, I. (1986) Leakage of periplasmic proteins from Escherichia coli mediated by polymyxin B nonapeptide. *Antimicrob. Agents Chemother.* **29**, 781-788
36. Sahalan, A. Z., and Dixon, R. A. (2008) Role of the cell envelope in the antibacterial activities of polymyxin B and polymyxin B nonapeptide against Escherichia coli. *Int. J. Antimicrob. Agents* **31**, 224-227
37. Wiese, A., Münstermann, M., Gutsmann, T., Lindner, B., Kawahara, K., Zähringer, U., and Seydel, U. (1998) Molecular Mechanisms of Polymyxin B-Membrane Interactions: Direct Correlation Between Surface Charge Density and Self-Promoted Transport. *J. Membr. Biol.* **162**, 127-138
38. Schroeder, G., Brandenburg, K., and Seydel, U. (1992) Polymyxin B induces transient permeability fluctuations in asymmetric planar lipopolysaccharide/phospholipid bilayers. *Biochemistry* **31**, 631-638
39. Hancock, R. E. W., and Chapple, D. S. (1999) Peptide Antibiotics. *Antimicrob. Agents Chemother.* **43**, 1317-1323
40. Alba, B. M., and Gross, C. A. (2004) Regulation of the Escherichia coli σ E-dependent envelope stress response. *Mol. Microbiol.* **52**, 613-619
41. Lima, S., Guo, M. S., Chaba, R., Gross, C. A., and Sauer, R. T. (2013) Dual Molecular Signals Mediate the Bacterial Response to Outer-Membrane Stress. *Science* **340**, 837-841
42. Hagan, C. L., Silhavy, T. J., and Kahne, D. (2011) ß-Barrel membrane protein assembly by the Bam complex. *Annu. Rev. Biochem.* **80**, 189-210

Downloaded from http://www.jbc.org/ at UZH Hauptbibliothek / Zentralbibliothek Zuerich on February 8, 2016

43. Zhang, G., Meredith, T. C., and Kahne, D. (2013) On the essentiality of lipopolysaccharide to Gram-negative bacteria. *Curr. Opin. Microbiol.* **16**, 779-785
44. Whitfield, C., and Trent, M. S. (2014) Biosynthesis and export of bacterial lipopolysaccharides. *Annu. Rev. Biochem.* **83**, 99-128
45. Gogol, E. B., Rhodius, V. A., Papenfort, K., Vogel, J., and Gross, C. A. (2011) Small RNAs endow a transcriptional activator with essential repressor functions for single-tier control of a global stress regulon. *Proc. Natl. Acad. Sci. USA* **108**, 12875-12880
46. Guo, M. S., Updegrove, T. B., Gogol, E. B., Shabalina, S. A., Gross, C. A., and Storz, G. (2014) MicL, a new sigma(E)-dependent sRNA, combats envelope stress by repressing synthesis of Lpp, the major outer membrane lipoprotein. *Genes Dev.* **28**, 1620-1634
47. Majdalani, N., and Gottesman, S. (2005) The Rcs phosphorelay: A Complex Signal Transduction System. *Annu. Rev. Microbiol.* **59**, 379-405
48. Gottesman, S., and Stout, V. (1991) Regulation of capsular polysaccharide synthesis in Escherichia coli K12. *Mol. Microbiol.* **5**, 1599-1606
49. Bader, M. W., Navarre, W. W., Shiau, W., Nikaido, H., Frye, J. G., McClelland, M., Fang, F. C., and Miller, S. I. (2003) Regulation of Salmonella typhimurium virulence gene expression by cationic antimicrobial peptides. *Mol. Microbiol.* **50**, 219-230
50. Dalebroux, Z. D., and Miller, S. I. (2014) Salmonellae PhoPQ regulation of the outer membrane to resist innate immunity. *Curr. Opin. Microbiol.* **17**, 106-113
51. Raetz, C. R. H., Reynolds, C. M., Trent, M. S., and Bishop, R. E. (2007) Lipid A Modification Systems in Gram-Negative Bacteria. *Annu. Rev. Biochem.* **76**, 295-329
52. Boehm, A., Steiner, S., Zaehringer, F., Casanova, A., Hamburger, F., Ritz, D., Keck, W., Ackermann, M., Schirmer, T., and Jenal, U. (2009) Second messenger signalling governs Escherichia coli biofilm induction upon ribosomal stress. *Mol. Microbiol.* **72**, 1500-1516
53. Hayden, J. D., and Ades, S. E. (2008) The Extracytoplasmic Stress Factor, σE, Is Required to Maintain Cell Envelope Integrity in Escherichia coli. *PLoS ONE* **3**, e1573
54. Koike, M., Iida, K., and Matsuo, T. (1969) Electron microscopic studies on mode of action of polymyxin. *J. Bacteriol.* **97**, 448-452
55. Deris, Z. Z., Swarbrick, J. D., Roberts, K. D., Azad, M. A. K., Akter, J., Horne, A. S., Nation, R. L., Rogers, K. L., Thompson, P. E., Velkov, T., and Li, J. (2014) Probing the Penetration of Antimicrobial Polymyxin Lipopeptides into Gram-Negative Bacteria. *Bioconj. Chem.* **25**, 750-760
56. Whitfield, C. (2006) Biosynthesis and assembly of capsular polysaccharides in *Escherichia coli*. *Annu. Rev. Biochem.* **75**, 39-68
57. Sperandeo, P., Cescutti, R., Villa, R., Di Benedetto, C., Candia, D., Dehò, G., and Polissi, A. (2007) Characterization of lptA and lptB, Two Essential Genes Implicated in Lipopolysaccharide Transport to the Outer Membrane of Escherichia coli. *J. Bacteriol.* **189**, 244-253
58. Sperandeo, P., Lau, F. K., Carpentieri, A., De Castro, C., Molinaro, A., Dehò, G., Silhavy, T. J., and Polissi, A. (2008) Functional Analysis of the Protein Machinery Required for Transport of Lipopolysaccharide to the Outer Membrane of Escherichia coli. *J. Bacteriol.* **190**, 4460-4469
59. Wu, T., McCandlish, A. C., Gronenberg, L. S., Chng, S.-S., Silhavy, T. J., and Kahne, D. (2006) Identification of a protein complex that assembles lipopolysaccharide in the outer membrane of Escherichia coli. *Proc. Natl. Acad. Sci. USA* **103**, 11754-11759

Downloaded from http://www.jbc.org/ at UZH Hauptbibliothek / Zentralbibliothek Zuerich on February 8, 2016

60. Doerrler, W. T., Reedy, M. C., and Raetz, C. R. H. (2001) An Escherichia coli mutant defective in lipid export. *J. Biol. Chem.* **276**, 11461-11464
61. Dong, C., Beis, K., Nesper, J., Brunkan-LaMontagne, A. L., Clarke, B. R., Whitfield, C., and Naismith, J. H. (2006) Wza the translocon for E. coli capsular polysaccharides defines a new class of membrane protein. *Nature* **444**, 226-229
62. Dunstan, R. A., Hay, I. D., Wilksch, J. J., Schittenhelm, R. B., Purcell, A. W., Clark, J., Costin, A., Ramm, G., Strugnell, R. A., and Lithgow, T. (2015) Assembly of the secretion pores GspD, Wza and CsgG into bacterial outer membranes does not require the Omp85 proteins BamA or TamA. *Mol. Microbiol.* **97**, 616-629
63. Lyu, Z. X., and Zhao, X. S. (2015) Periplasmic quality control in biogenesis of outer membrane proteins. *Biochem. Soc. Trans.* **43**, 133-138
64. Smit, J., and Nikaido, H. (1978) Outer membrane of gram-negative bacteria. XVIII. Electron microscopic studies on porin insertion sites and growth of cell surface of Salmonella typhimurium. *J. Bacteriol.* **135**, 687-702
65. Mühlradt, P. F., Menzel, J., Golecki, J. R., and Speth, V. (1974) Lateral Mobility and Surface Density of Lipopolysaccharide in the Outer Membrane of Salmonella typhimurium. *Eur. J. Biochem.* **43**, 533-539
66. Ursell, T. S., Trepagnier, E. H., Huang, K. C., and Theriot, J. A. (2012) Analysis of Surface Protein Expression Reveals the Growth Pattern of the Gram-Negative Outer Membrane. *PLoS Comput. Biol.* **8**, e1002680
67. Rassam, P., Copeland, N. A., Birkholz, O., Toth, C., Chavent, M., Duncan, A. L., Cross, S. J., Housden, N. G., Kaminska, R., Seger, U., Quinn, D. M., Garrod, T. J., Sansom, M. S. P., Piehler, J., Baumann, C. G., and Kleanthous, C. (2015) Supramolecular assemblies underpin turnover of outer membrane proteins in bacteria. *Nature* **523**, 333-340
68. Gessmann, D., Chung, Y. H., Danoff, E. J., Plummer, A. M., Sandlin, C. W., Zaccai, N. R., and Fleming, K. G. (2014) Outer membrane beta-barrel protein folding is physically controlled by periplasmic lipid head groups and BamA. *Proc. Natl. Acad. Sci. USA* **111**, 5878-5883
69. Lepore, B. W., Indic, M., Pham, H., Hearn, E. M., Patel, D. R., and van den Berg, B. (2011) Ligand-gated diffusion across the bacterial outer membrane. *Proc. Natl. Acad. Sci. USA* **108**, 10121-10126
70. Albrecht, R., Schutz, M., Oberhettinger, P., Faulstich, M., Bermejo, I., Rudel, T., Diederichs, K., and Zeth, K. (2014) Structure of BamA, an essential factor in outer membrane protein biogenesis. *Acta Cryst. Sect. D-Biol. Cryst.* **70**, 1779-1789
71. Ni, D. C., Wang, Y., Yang, X., Zhou, H. Z., Hou, X. M., Cao, B. H., Lu, Z. X., Zhao, X. S., Yang, K., and Huang, Y. H. (2014) Structural and functional analysis of the beta-barrel domain of BamA from Escherichia coli. *Faseb Journal* **28**, 2677-2685
72. Noinaj, N., Kuszak, A. J., Gumbart, J. C., Lukacik, P., Chang, H. S., Easley, N. C., Lithgow, T., and Buchanan, S. K. (2013) Structural insight into the biogenesis of beta-barrel membrane proteins. *Nature* **501**, 385-390
73. Noinaj, N., Kuszak, A. J., Balusek, C., Gumbart, J. C., and Buchanan, S. K. (2014) Lateral Opening and Exit Pore Formation Are Required for BamA Function. *Structure* **22**, 1055-1062
74. Dong, H. H., Xiang, Q. J., Gu, Y. H., Wang, Z. S., Paterson, N. G., Stansfeld, P. J., He, C., Zhang, Y. Z., Wang, W. J., and Dong, C. J. (2014) Structural basis for outer membrane lipopolysaccharide insertion. *Nature* **511**, 52-56

Downloaded from http://www.jbc.org/ at UZH Hauptbibliothek / Zentralbibliothek Zuerich on February 8, 2016

75. Qiao, S., Luo, Q. S., Zhao, Y., Zhang, X. J. C., and Huang, Y. H. (2014) Structural basis for lipopolysaccharide insertion in the bacterial outer membrane. *Nature* **511**, 108-111

Downloaded from http://www.jbc.org/ at UZH Hauptbibliothek / Zentralbibliothek Zuerich on February 8, 2016

Figure Legends

Figure 1. **Structure and effects of JB-95 on *E. coli***. **A**, Structure of JB-95. The fluorescence probe flJB-95 contains the residue B in place of Arg^9 (dotted box); The photoprobe PAL-95 contains residue Z in place of Arg^9 and L-photoproline (dotted box) in place of L-Pro^{14}. **B,** Kinetics of killing of *E. coli* ATCC25922 in microplate format by JB-95 and protegrin-I in LB (control = no antibiotic). **C**, Fluorescence increase of *E. coli* cells treated with polymyxin B or JB-95 in the presence of SYTOX green. Control with cells and SYTOX and no antibiotic is included. **D**, Relative incorporation of ^{3}H-label from [1,6-^{3}H]-N-acetylglucosamine (♦) and [2,6-^{3}H]-diaminopimelic acid (◊) into macromolecules in *E. coli* over 20 min at 37ºC with increasing concentrations of JB-95 (the vertical dotted line corresponds to the MIC), showing the stimulated incorporation of label from N-acetylglucosamine. (All results in triplicate with error bars).

Figure 2. Solution structure of JB-95. **A**, the blue arrows indicate long range NOEs seen in 2D ^{1}H-NMR NOESY and ROESY spectra. **B**, Superimposition and representation of the backbone atoms of the final 20 NMR structures of JB-95. Side chains omitted for clarity. O-atoms, red; N-atoms, blue. The D-Pro-L-Pro template is shown to the right in pink. **C**, one typical average solution structure of JB-95.

Figure 3. Fluorescence microscopy of *E. coli* cells. *E. coli* ATCC25922 cells grown in MH-II without drug and stained with SYTOX Green, DAPI and FM-4-64 (panel **A**) and cells treated with either JB-95 (5 μg/ml, **B-E**) or polymyxin B (PMB, 0.03μg/ml, **F-H**) for 1 h at 30ºC and labeled with fluorescent dye, were analyzed using a Leica CLSM SP8 gSTED microscope (scale bar 4 μm). Images shown: **A**, control cells, no drug; with **JB-95**, **B**, SYTOX Green staining (no signal visible), **C**, DAPI staining, **D**, FM4-64 staining, **E**, superimposition of **B-D**; with **PMB**, **F**, FM4-64 staining, **G**, SYTOX Green staining, **H**, superimposition of **F-G**; **I**, cells stained with flJB-95 (see Figure 1A) for 30 min in MH broth.

Figure 4. **TEM (A-D) and SEM (E-F) studies of JB-95 treated cells**. *E. coli* ATCC25922 was grown in shake cultures in LB medium with JB-95 concentrations that cause ≈ 50% growth inhibition. **A**, control, untreated (no drug). **B** and **C**, Cells grown with JB-95 (10 μg/ml), showing breaks in the OM (arrow). **D**, Accumulations of membrane-like material in the periplasm of JB-95-treated cells (arrow). The OM is also indicated. **E**, SEM of cells without antibiotic and **F**, grown with JB-95 (10 μg/ml) showing knob-like protuberances on the surface. Scale bars (white/black) = 200 nm.

Figure 5. Permeability effects caused by JB-95 on *E. coli* cells. A, *E. coli* grown in LB with JB-95 (5 μg/ml, causing 50% inhibition), adjusted to OD_{600}=1 and plated at increasing dilutions onto LB agar (*left*), or LB + EDTA (0.5 mM) + SDS (0.5%) (*right*). Cells are much more sensitive to SDS/EDTA after treatment with JB-95. **B/C**, ß-Lactamase assay. Cells were treated with JB-95 (blue), polymyxin (red) or ciprofloxacin (brown) (untreated, green) and ß-lactamase

Downloaded from http://www.jbc.org/ at UZH Hauptbibliothek / Zentralbibliothek Zuerich on February 8, 2016

release was assayed with CENTA. **B**, kinetics of ß-lactamase release at the concentrations shown; **C**, dose-response curves relative to untreated cells. **D**, ß-Galactosidase assay. Cells treated with JB-95 do not release ß-galactosidase from the cytoplasm, whereas PMB and PG-I cause release. Dose-responses are shown, with green dotted line = 100% release (lysed cells).

Figure 6. **Proteomics studies**. **A**, SDS-PAGE of the membrane extract from treated (+) and untreated (-) *E. coli* ATCC25922, showing depletion of some OM proteins in treated cells. **B**, Differential protein expression analysis. The $\log_2$ fold change in the induced (I, with JB-95) versus un-induced (U, no JB-95) membrane proteome shown against mean normalized spectral count, analyzed using DESeq2. The most significantly differentially expressed proteins are highlighted with red/green dots, and are listed in Table-2.

Figure 7. **Photolabeling experiment with PAL-95**. **A,** Western blot with chemiluminescence detection of biotinylated proteins. OM proteins from *E. coli* cells photolabeled with PAL-95 (Figure 1A) were separated by 2D electrophoresis, blotted to a PVDF membrane and biotinylated proteins were detected by chemiluminescence. The unique positions of labeled BamA (≈95 kDa) and LptD (≈98 and 130 kDa) in the 2D gels allow unambiguous identification of these labeled proteins in the blots. LptD (oxidized) appears at ≈130 kDa, and LptD (reduced) at ≈98kDa. **B,** Coomassie stained 2D gel of the OM proteins extracted from *E. coli*.

Downloaded from http://www.jbc.org/ at UZH Hauptbibliothek / Zentralbibliothek Zuerich on February 8, 2016

Table-1.

Antimicrobial activities. The MICs (μg/ml) were measured using the broth micro-dilution assay. The six non-ATCC *E. coli* strains are clinical isolates showing drug resistance to the antibiotics shown. nd = not determined.

mimetic/test organism	*E. coli* ATCC25922	*A. baumanii* ATCC17978	*P. aeruginosa* ATCC27853	*S. aureus* ATCC29213
JB-95	0.25	1	4	2
ent-JB-95	1	4	8	4
PAL-95	0.5	nd	nd	nd
flJB-95	4	nd	nd	nd

strain/ antibiotic	*E. coli* ATCC 25922	*E. coli* 2138E/ 2151	*E. coli* 2139E/ 2152	*E. coli* 2140E/ 2153	*E. coli* 2143E/ 2154	*E. coli* 2144E/ 2155	*E. coli* 3459/ 2150
JB-95	0.25	0.25	0.25	0.25	0.25	0.5	0.25
colistin	0.12	0.12	0.03	0.06	0.06	16	0.06
gentamycin	0.5	1	0.5	8	1	0.06	1
ceftriaxone	0.06	0.06	0.06	0.06	0.12	1	>64
ampicillin	16	>64	>64	>64	>64	0.12	>64
rifampicin	32	64	64	64	>64	0.12	8
erythromycin	>64	>64	64	64	64	0.12	>64
azithromycin	8	8	4	8	4	1	4
ciprofloxacin	0.008	0.12	0.02	0.01	0.02	0.25	0.12

Downloaded from http://www.jbc.org/ at UZH Hauptbibliothek / Zentralbibliothek Zuerich on February 8, 2016

Table-2.

Differential membrane protein analysis. Semi-quantitative changes in 56 *E. coli* ATCC25922 proteins that showed significant differential expression after JB-95 addition (I), compared to untreated cells (U). The $\log_2$(I/U)-fold change in expression is shown (DESeq analysis q-value ≤ 0.06). PSORTb predicted OM proteins are highly enriched among differentially expressed proteins (P-value < 10^{-15}), and except the product of *wza*, are all down-regulated. Wza does not have a ß-barrel topology, but rather a transmembrane domain of eight α-helices (61).

Class	Locus ID[a]	Localization[b]	BOMP predict -ion[c]	Description[a]	Gene name	$\log_2$ Fold change I vs U[d]
Energy production and conversion	EG10095	Cytoplasmic		L-Aspartate ammonia-lyase	*aspA*	-2.3
	EG10232	CM		DMSO reductase subunit A	*dmsA*	-3.2
	EG10233	Unknown		DMSO reductase subunit B	*dmsB*	-2.9
	EG10330	CM		Fumarate reductase flavoprotein subunit	*frdA*	-2.2
	EG10331	CM		Fumarate reductase iron-sulfur protein subunit	*frdB*	-1.9
	EG10393	CM		Anaerobic glycerol-3-phosphate dehydrogenase	*glpC*	-3.0
	EG10701	Cytoplasmic		Formate C-acetyltransferase; pyruvate formate-lyase	*pflB*	-1.4
	EG11227	Periplasmic		Formate dehydrogenase-N	*fdnG*	-2.3
	EG11801	CM		Hydrogenase-2 large subunit	*hybC*	-2.6
	EG13006	CM		Hydrogenase-2 small subunit	*hybO*	-2.4
	EG13844	CM		S- and N-oxide reductase, A subunit	*ynfF*	-3.9
Amino Acid metabolism and transport	EG10674	Periplasmic		Oligopeptide-binding protein	*oppA*	-2.7
	EG11005	Cytoplasmic		Tryptophanase	*tnaA*	-1.6
	EG10386	Periplasmic		Glutamine-binding protein	*glnH*	-2.5
Nucleotide metabolism and transport	EG12130	Cytoplasmic		DnaK-like chaperone Hsc66	*hscA*	3.4
Carbohydrate metabolism and transport	EG10283	Cytoplasmic		Fructose-1,6-bisphosphatase	*fbp*	2.9
	EG10528	OM	4	Maltoporin, maltose high-affinity uptake system	*lamB*	-3.0
	EG10560	Cytoplasmic		Maltodextrin phosphorylase	*malP*	-2.5
Coenzyme metabolism	EG10432	Cytoplasmic		Glutamate-1-semialdehyde aminomutase	*hemL*	2.3
Lipid metabolism	EG10280	OM	5	Fatty acid transport protein	*fadL*	-2.3
Cell wall, membrane, envelope biogenesis	EG10669	OM	1	Outer membrane protein A	*ompA*	-2.0
	EG10670	OM	5	Outer membrane porin C	*ompC*	-2.7
	EG10671	OM	5	Outer membrane porin F	*ompF*	-2.7
	EG10738	OM	4	Outer-membrane phospholipase A	*pldA*	-3.2
	EG11035	OM	3	Outer membrane channel for nucleosides	*tsx*	-2.5
	EG11124	OM	4	Outer membrane protein W	*ompW*	-3.0
	EG11569	OM	1	LPS assembly complex LptD/E	*lptD*	-3.2
	EG11787	Cytoplasmic		Fucose biosynthesis; GDP-D-mannose 4,6-dehydratase	*gmd*	3.5
	EG11790	Cytoplasmic		Putative colanic acid biosynthesis glycosyl transferase	*wcaI*	3.2
	EG12135	OM	5	Outer membrane protein X	*ompX*	-1.8
	EG12513	OM	1	Assembly module for autotransporter export	*tamA*	-4.1
	EG13492	OM	5	MltA-interacting protein	*mipA*	-3.1
	EG13566	OM	2	Colanic acid export channel lipoprotein	*wza*	3.5
	EG13568	CM		Tyrosine-protein kinase; colanic acid production	*wzc*	4.3
	EG14090	CM		Undecaprenyl phosphate-aminoarabinose synthase	*arnC*	1.9
	EG14091	Cytoplasmic		UDP-glucuronate dehydrogenase	*arnA*	3.1
Cell motility	EG10321	Extracellular		Flagellin, structural gene, H-antigen	*fliC*	-3.0
Post translational modifications	EG10159	Cytoplasmic		ATPase subunit of ClpXP protease	*clpX*	2.0

Downloaded from http://www.jbc.org/ at UZH Hauptbibliothek / Zentralbibliothek Zuerich on February 8, 2016

	EG10463	Periplasmic		Periplasmic, membrane-associated serine endoprotease	*degP*	2.1
Inorganic ion transport and metabolism	EG10014	CM		Aminoglycoside efflux pump; RND-type transporter	*acrD*	3.7
	EG10126	OM	3	Vitamin B12 outer membrane receptor	*btuB*	-4.1
	EG10286	OM	1	OM ferric citrate receptor	*fecA*	-4.9
	EG10302	OM	4	OM transporter for ferrichrome-iron	*fhuA*	-3.3
	EG10514	CM		Potassium-translocating ATPase, B subunit	*kdpB*	3.8
	EG12525	CM		Magnesium transporter, ATP-dependent	*mgtA*	4.5
	EG13774	OM	1	Putative TonB-dependent OM receptor	*yncD*	-3.6
	EG10260	Cytoplasmic		Isochorismatase, aryl carrier protein (ArCP)	*entB*	3.6
Signal transduction	EG10732	CM		Histidine protein kinase sensor protein	*phoQ*	2.4
	EG11233	CM		Sensory histidine kinase of RstAB two-component system	*rstB*	3.1
Intracellular trafficking and secretion	EG11009	OM	0	OM factor (OMF) of tripartite efflux pumps	*tolC*	-2.3
	EG12686	OM		Antigen 43, phase-variable bipartite OM protein	*flu*	-2.5
Others	EG10988	CM		Aspartate, maltose chemoreceptor, methyl-accepting	*tar*	-3.2
	EG11613	CM		Lipid A phosphoethanolamine transferase	*eptA*	1.8
	EG12257	Unknown		Oxidase involved in cellulose production	*bcsC*	-3.9
	EG13693	Unknown		DUF535 family protein, function unknown	*ybjX*	4.5
	EG13929	Unknown		DUF1471 family periplasmic tri-domain protein	*ydgH*	-4.0

[a]Gene number and nomenclature according to Ecogene 3.0

[b]Localization identified as described in the Methods section (CM=cytoplasmic membrane; OM=outer membrane)

[c]Beta-barrel OM protein (BOMP) identified as described in the Methods section (0 = did not find the protein to be an integral OM protein, but there were integral OM homologs, 1 = least reliable prediction, and 5 = most reliable prediction)

[d] $\log_2$ fold change of protein expression, comparing induced cells (I, with JB-95) and un-induced (U, no drug).

Downloaded from http://www.jbc.org/ at UZH Hauptbibliothek / Zentralbibliothek Zuerich on February 8, 2016

Figure 1

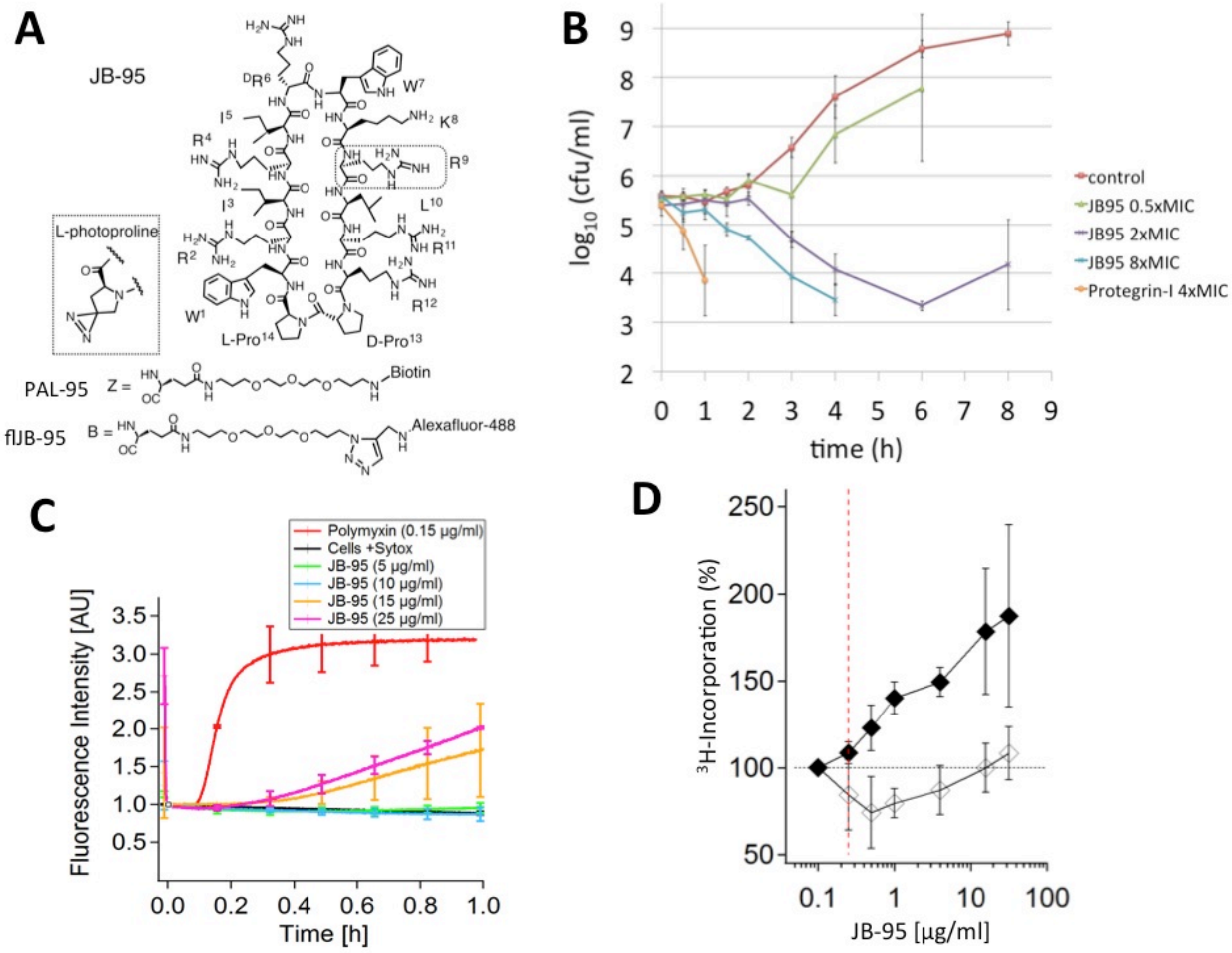

Downloaded from http://www.jbc.org/ at UZH Hauptbibliothek / Zentralbibliothek Zuerich on February 8, 2016

Figure 2

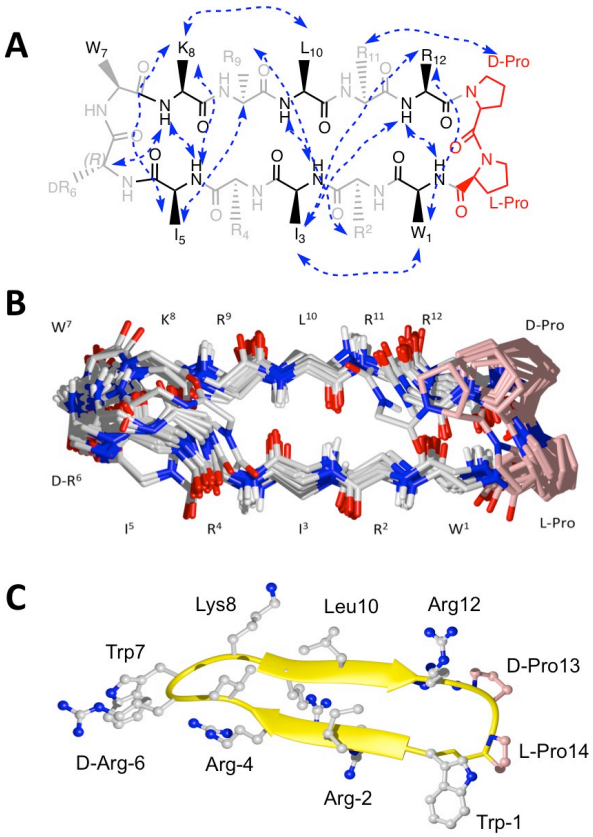

Downloaded from http://www.jbc.org/ at UZH Hauptbibliothek / Zentralbibliothek Zuerich on February 8, 2016

Figure 3

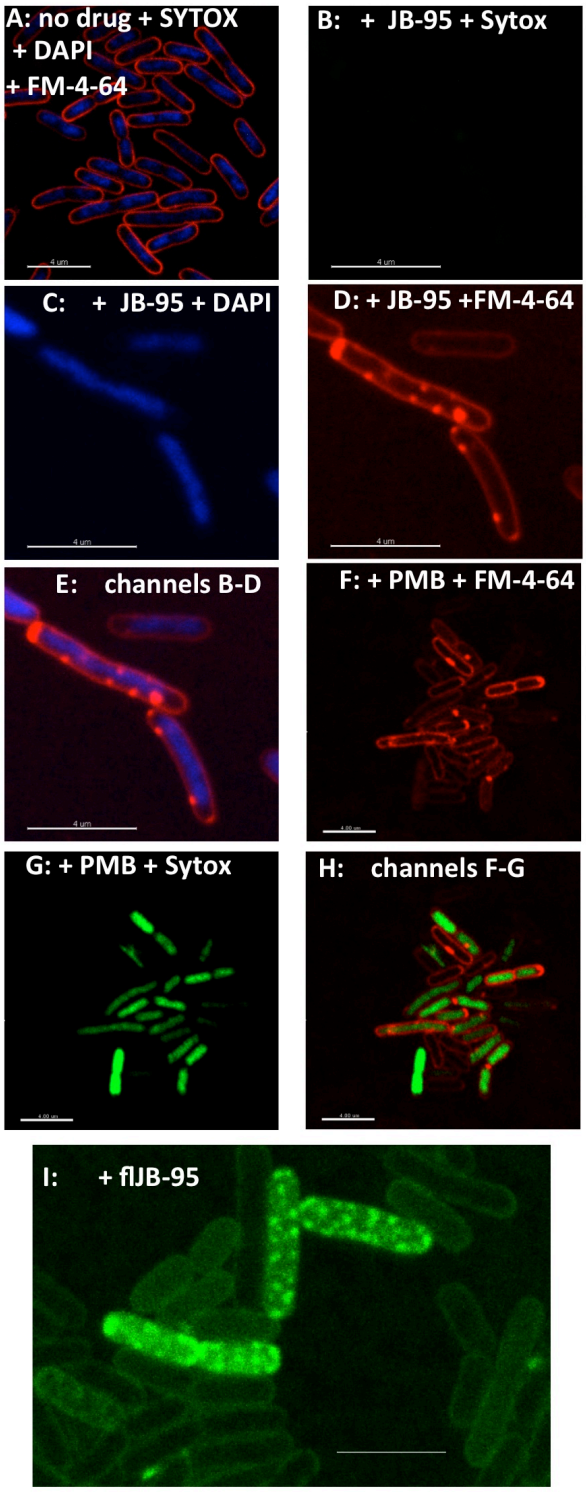

Downloaded from http://www.jbc.org/ at UZH Hauptbibliothek / Zentralbibliothek Zuerich on February 8, 2016

Figure 4

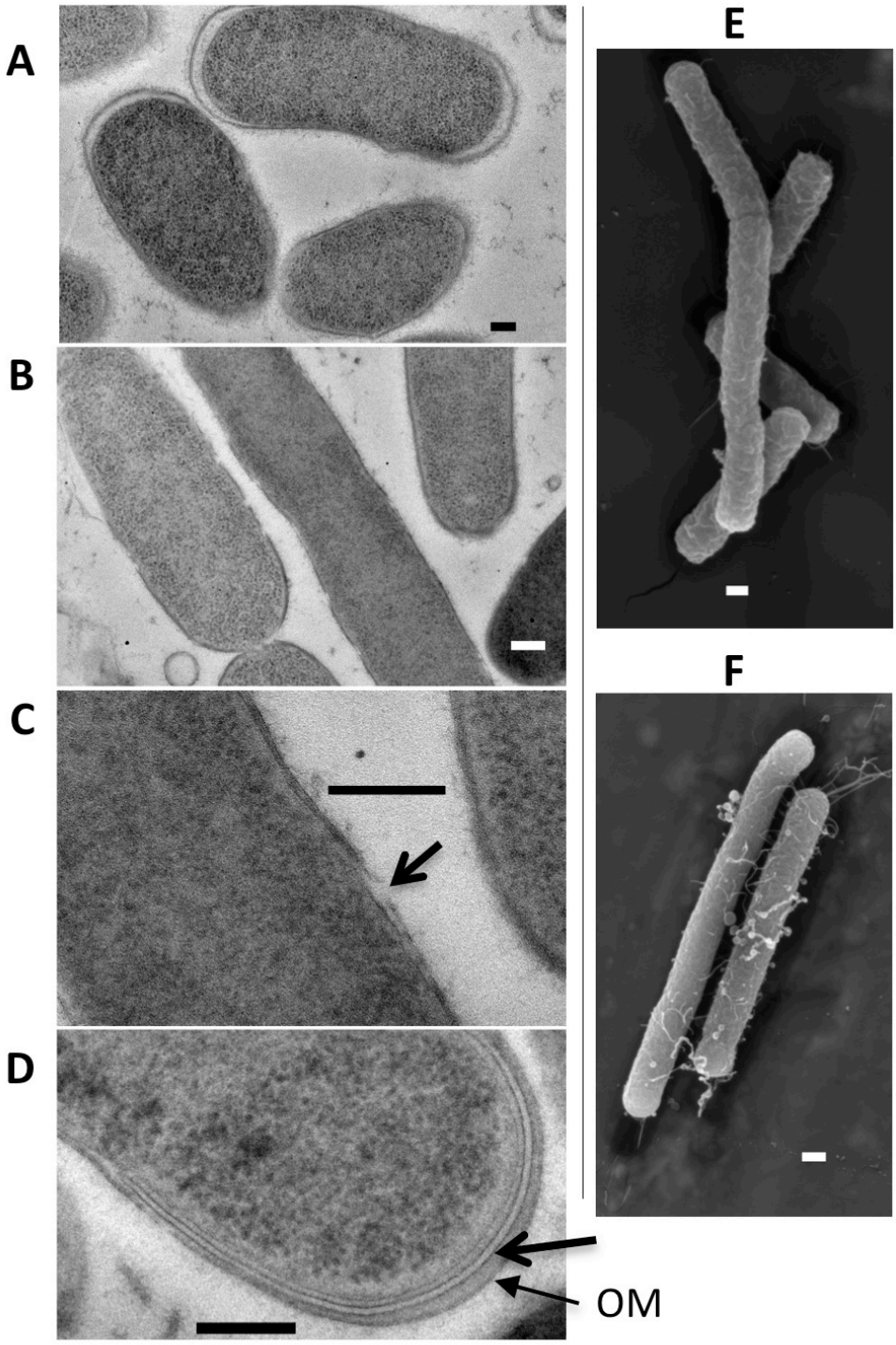

Downloaded from http://www.jbc.org/ at UZH Hauptbibliothek / Zentralbibliothek Zuerich on February 8, 2016

Figure 5

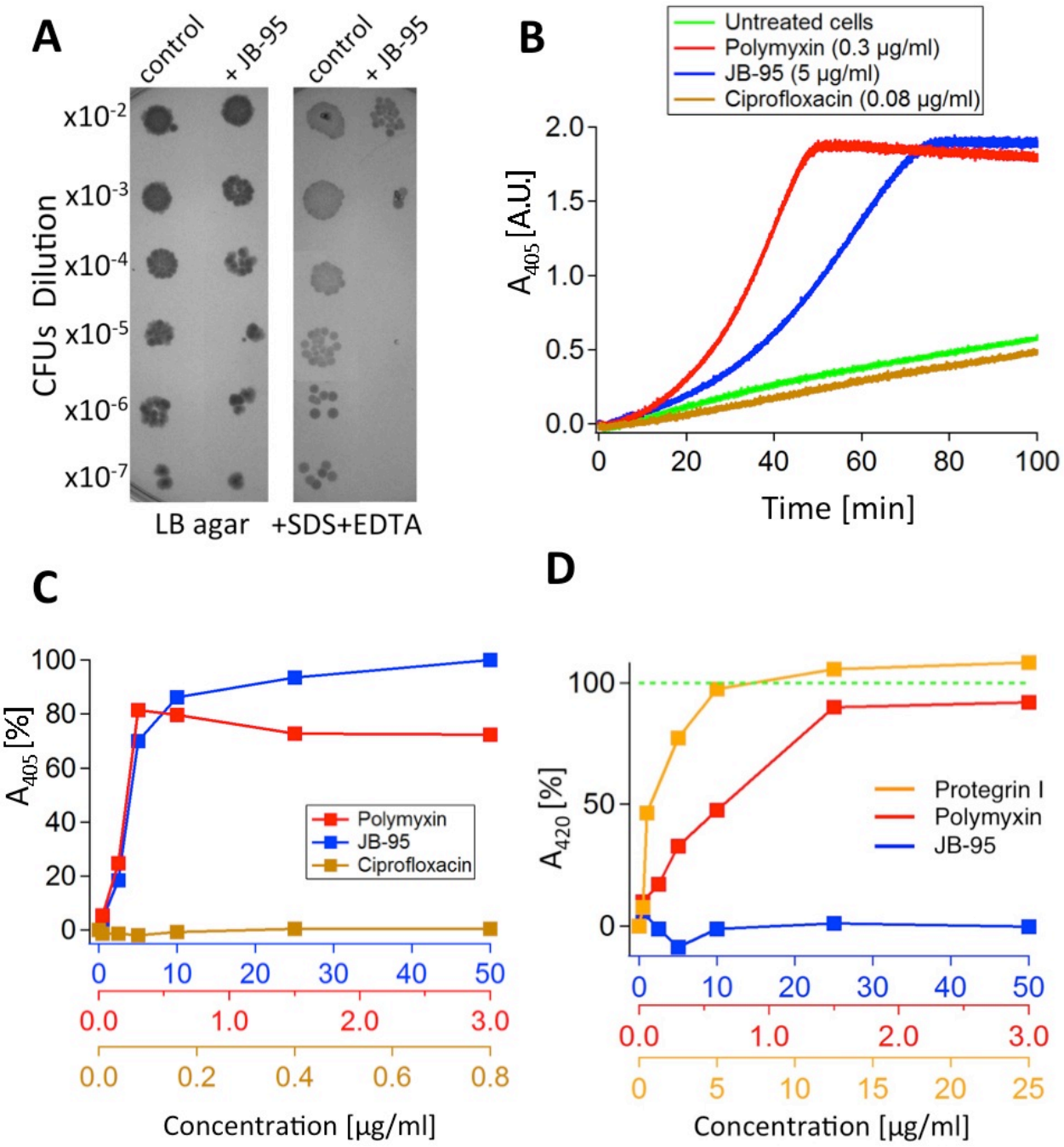

Downloaded from http://www.jbc.org/ at UZH Hauptbibliothek / Zentralbibliothek Zuerich on February 8, 2016

Figure 6

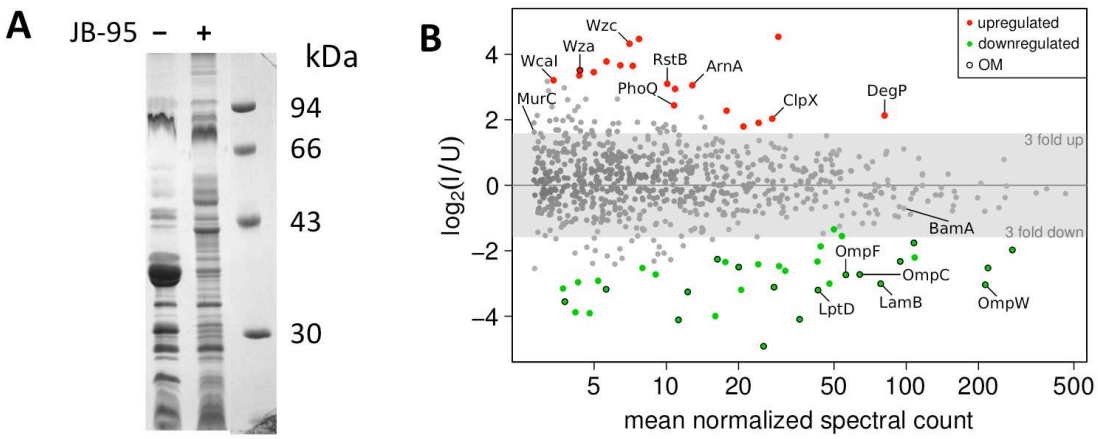

Downloaded from http://www.jbc.org/ at UZH Hauptbibliothek / Zentralbibliothek Zuerich on February 8, 2016

Figure 7

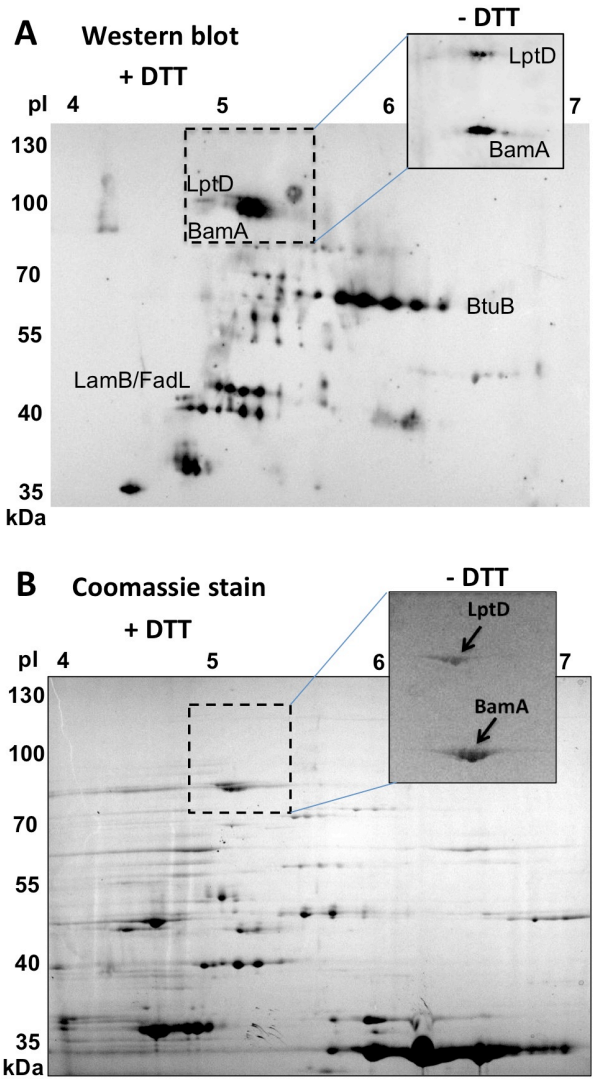

Downloaded from http://www.jbc.org/ at UZH Hauptbibliothek / Zentralbibliothek Zuerich on February 8, 2016

Supporting Information

A Peptidomimetic Antibiotic Targets Outer Membrane Proteins and Disrupts Selectively the Outer Membrane in *Escherichia coli*

1. Peptide synthesis.

2. NMR studies of the solution conformation of JB-95

3. qPCR primers

1. Peptide synthesis.

Synthesis of the fluorescence probe flJB-95.
The following synthetic route to the fluorescently labelled flJB-95 was followed:

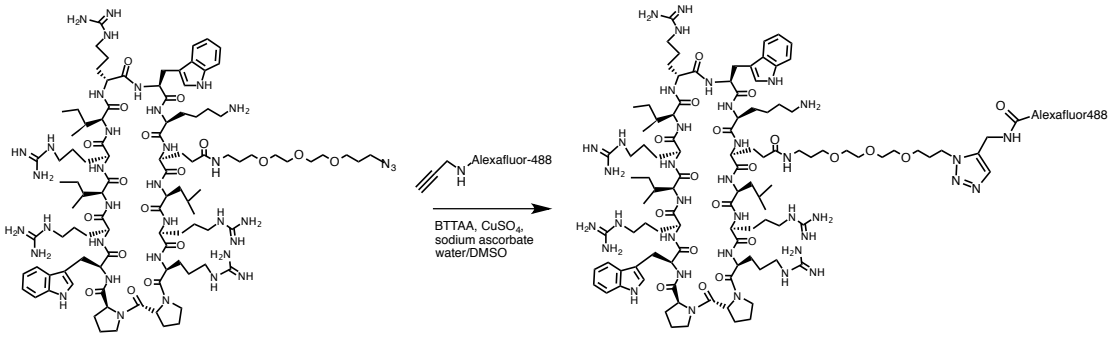

The cyclic peptide precursor was prepared by solid-phase assembly of a linear peptide precursor followed by macrocyclization in solution, using methods described earlier (1). Standard Fmoc-protected amino acids and Fmoc-Glu(PEG-N_3)-OH were used for solid-phase peptide synthesis.

To the cyclic peptide (1.37 mg) in PBS (700 μL) was added BTTAA (2-[4-{(bis[(1-tert-butyl-1*H*-1,2,3-triazol-4-yl)methyl]amino)methyl}-1*H*-1,2,3-triazol-1-yl]acetic acid(2)) (0.82 mg), sodium ascorbate (0.1 M, 30 μL), AlexaFluor-488 alkyne (0.25 mg, *Molecular Probes, Inc*.) in DMSO (100 μL) and $CuSO_4$ (0.1 M, 30 μL). After 1 h another aliquot of sodium ascorbate (0.1 M, 30 μL) and $CuSO_4$ (0.1 M, 30 μL) was added and stirred for another 1 h. The reaction was quenched by addition of water (1 mL) containing 0.1% TFA. The product was purified by reversed phase HPLC on an Agilent Eclipse XDB-C18 semi-preparative column employing a MeCN/H_2O gradient with 0.1% TFA. Yield 0.6 mg of an orange powder, 95% purity by reverse phase HPLC. Retention time = 9.55 min (*Grace* VYDAC® 218TP54, C18 column, 5 μm, 4.6x250 mm, flow 1 ml/min, gradient 20-60% MeCN/H_2O +0.1% TFA over 6 column volumes. High resolution ES-MS: *m/z* 679.58826 ($M+4H^+$), calc. mass 679.58786.

2. NMR Studies of the Solution Conformation of JB-95

^{1}H NMR measurements were performed either in H_2O/D_2O (9:1) or pure D_2O at pH 5.6 and pH 3. Spectra were acquired on a Bruker AV-600 spectrometer at 300 K. 1D and 2D TOCSY ^{1}H NMR spectra were also recorded at various temperatures (280 K, 290 K, 310 K and 320 K) for determination of the amide temperature coefficients. Water suppression was performed by presaturation. ^{1}H-NMR assignments (given below) were made using 2D DQF-COSY, TOCSY, NOESY and ROESY spectra. All spectra were referenced on internal trimethylsilyl propanoic acid (TSP).

^{1}H Chemical shifts of JB-95 in 90% H_2O/10%D_2O, pH 5, 300 K.

	NH	H-C(α)	H-C(β)	Others
Trp[1]	7.87	4.88	3.31, 3.31	H(δ^1) 7.36; H(ε^3) 7.74; H(ζ^2) 7.52; H(ζ^3) 7.13; H(η^2) 7.27; NH(ε^1) 10.24
Arg[2]	8.75	4.96	1.72,1.80	CH_2(γ) 1.51, 1.64; CH_2(δ) 3.13, 3.16; NH(ε) 7.22; NH_2(η) -, -
Ile[3]	8.65	4.50	1.77	$CH_2(\gamma^1)$ 1.03, 1.31; $CH_3(\gamma^2)$ 0.83; $CH_3(\delta^1)$ 0.80
Arg[4]	8.56	5.04	1.60, 1.77	CH_2(γ) 1.39, 1.46; CH_2(δ) 3.15, 3.15; NH(ε) 7.16; NH_2(η) -, -
Ile[5]	8.37	4.17	1.68	$CH_2(\gamma^1)$ 1.03, 1.38; $CH_3(\gamma^2)$ 0.83; $CH_3(\delta^1)$ 0.80
DArg[6]	8.81	3.99	1.38, 1.52	CH_2(γ) 0.40, 1.07; CH_2(δ) 2.85, 2.85; NH(ε) 6.78; NH_2(η) -, -
Trp[7]	8.93	4.90	3.10, 3.61	H(δ^1) 7.27; H(ε^3) 7.68; H(ζ^2) 7.51; H(ζ^3) 7.13; H(η^2) 7.26; NH(ε^1) 10.15
Lys[8]	8.14	4.52	1.85, 1.85	CH_2(γ) 1.38, 1.46; CH_2(δ) 1.71, 1.71; CH_2(ε) 3.01, 3.01; CH_3(ζ) -
Arg[9]	8.59	4.94	1.75, 1.75	CH_2(γ) 1.47, 1.65; CH_2(δ) 3.16, 3.16; NH(ε) 7.29; NH_2(η) -, -
Leu[10]	8.87	4.72	1.55, 1.61	CH(γ) 1.54; CH_3(δ) 0.88, 0.88
Arg[11]	8.63	4.93	1.76, 1.87	CH_2(γ) 1.52, 1.66; CH_2(δ) 3.18, 3.18; NH(ε) 7.23; NH_2(η) -, -
Arg[12]	8.74	4.90	1.73, 1.92	CH_2(γ) 1.62, 1.64; CH_2(δ) 3.17, 3.25; NH(ε) 7.23; NH_2(η) -, -
Dpro[13]	-	4.71	1.90, 2.28	CH_2(γ) 2.02, 2.14; CH_2(δ) 3.50, 3.87
Pro[14]		4.35	1.42, 1.95	CH_2(γ) 0.85, 1.65; CH_2(δ) 3.55, 3.64

$^3J_{HN\alpha}$ coupling constants were determined from 1D spectra or from 2D NOESY spectra by inverse Fourier transformation of in-phase multiplets. [^{13}C,^{1}H]-HSQC spectra at natural abundance were recorded in pure D_2O. Chemical shift deviations (CSDs) from statistical random coil values ($\Delta\delta=\delta_{obs}-\delta_{coil}$) for Hα, Cα and Cβ resonances were measured. In peptide segments of three or more consecutive residues with predominantly β-sheet conformations, positive Hα and Cβ CSDs (downfield shifts) in the range of > 0.1 ppm and > 0.5 ppm are expected, whereas negative Cα CSDs < 0.5 ppm are expected. The opposite trends apply to α-helical regions. $^3J_{HN^\alpha}$ values are correlated with the backbone torsion angle ϕ via the Karplus relation and should be < 6 Hz in α-helices and > 8 Hz in β-sheets. Amide proton temperature coefficients ($-\Delta\delta_{NH}/T$, ppb/K) are typically smaller than -4 to -5 ppb/K for amide protons that are shielded from solvent and/or are

involved in intramolecular hydrogen bond formation. Relative H/D exchange rates of amide protons are slowed when the NH is involved in intramolecular hydrogen bonding or otherwise shielded form solvent accessibility.

Cα and Cβ ^{13}C-chemical shifts for JB-95, $^{3}J_{HN\alpha}$(Hz) values, amide temperature coefficients (– Δδ/T (ppb/K)) and amide NH relative H/D exchange rates (+ slow, ++ medium, +++ fast) in 90% H_2O/10% D_2O, pH 5, 300 K.

	C(α)	C(β)	$^{3}J_{HN\alpha}$(Hz)	– Δδ/T (ppb/K)	rel. NH k_{exch}
Trp[1]	56.62	31.05	8.6	1.7	+
Arg[2]	55.48	31.46	8.6	7.7	+++
Ile[3]	59.81	41.71	9.4	3	+
Arg[4]	55.22	32.0	9.1	6.7	++
Ile[5]	60.4	39.30	9.5	2.1	+
D-Arg[6]	58.02	28.96	4.4	7.6	+++
Trp[7]	56.58	29.8	9.3	9	+++
Lys[8]	56.03	34.63	8.7	3	++
Arg[9]	55.45	31.57	9.1	7.1	+++
Leu[10]	54.28	45.1	9.0	2.9	+
Arg[11]	55.52	31.91	8.6	6.9	+++
Arg[12]	52.98	32.08	nd	2.4	+
D-pro[13]	61.42	30.73			
Pro[14]	63.68	32.17			

JB-95 appeared as a single species in solution, with *trans* peptide bonds. For example, a strong Hα-Hδ NOE was observed between Arg12-DPro13. The pattern of CSD values indicates a regular β-hairpin conformation with two extended β-strands between residues 1-5 and 8-12 characterized by positive ΔδHα, positive ΔδCβ and negative ΔδCα values. The strands are separated by a turn characterized by negative ΔδHα, negative ΔδCβ and positive ΔδCα values at DArg[6] and opposite CSD values at Trp[7]. These data are consistent with the formation of a type II' β-turn. $^{3}J_{NH\alpha C\alpha}$ coupling constants show large values >8 Hz except for residue 6 in the turn region, which is clear evidence for predominantly extended backbone conformations. Furthermore, H/D exchange experiments show slowly exchanging amide protons at Trp1, Ile3, Ile5, Lys8, Leu10 and Arg12. These residues are expected to occupy hydrogen-bonding positions in a regular β-hairpin register, due to intra-molecular hydrogen-bonding. The H/D exchange results correlate very well with the low NH temperature coefficients seen for these residues with values of < 4 ppb/K. The hydrogen bonds identified in these measurements were used as distance restraints in the calculation of the NMR-based structures.

Distance restraints were obtained from NOESY and ROESY spectra with a mixing time of 250 ms. The structure calculations were performed by restrained molecular dynamics in torsion angle space by applying the simulated annealing protocol implemented in the program DYANA (3). Starting from 100 randomized conformations a bundle of 20 conformations is selected, which incur the lowest DYANA target energy function. Well-ordered average solution structures could be determined based on numerous inter-strand NOEs in aqueous solution, which reveal a high population of β-hairpin conformations.

Characteristic backbone NOE connectivities of the β-hairpin fold could be observed in the NOESY spectrum between HN protons of Trp1-Arg12, Ile3-Leu10 and Ile5-Lys8. The calculated solution NMR structures converge to a narrow range of backbone conformations with an average rmsd to the mean structure of 0.9 Å. As assumed based on the CSD pattern in the tip region, a type II' β-turn was found with characteristic Hα-HN and HN-HN NOEs between DArg^{6}-Lys^{8} and Trp^{7}-Lys^{8}, respectively.

Statistics for the final 20 NMR structures calculated for JB-95 calculated using DYANA are given below.

	statisitics for JB-95
Number of NOE upper-distance limits	150
Intraresidue	80
Sequential	37
Medium- and long-range	33
Residual target function value (Å^2)	0.93 ± 0.18
Mean rmsd values (Å)	
All backbone atoms	1.32 ± 0.80
All heavy atoms	2.83 ± 1.01
Residual NOE violations	
Number > 0.2 Å	10
Maximum (Å)	0.34

3. qPCR primers

A list of primers used for qPCR analyses is given below.

Oligonucleotides used for qPCR.

Primer name	**Sequence (5' - 3')**
wcaI _F	TTCGCGTTCGATGATGAATA
wcaI _R	TTCACCAATATTGCCGGAGT
wzc _F	GATGTCGAGTCTGGTCAGCA
wzc _R	CAGCACACCCACGATAGAAA
murC _F	ATGGTTTCCAGCATCTACGC
murC _R	GTATCCATGTGGTCGGCTTC
arnA _F	CCGCCATTAAACACGGTAAT
arnA _R	CGACCAGACGGTGAATTTCT
ompF _F	AGGCTTTGGTATCGTTGGTG
ompF _R	AGCCGCTGGTGTTTGTAAAT
lptD _F	TGACAGTTCACGTCGTTGGT
lptD _R	GAAACGGTGGCATTGAAGTT
lamB _F	TGGTGGTTCTTCCTCTTTCG
lamB _R	GAATAACCAGCCGTCTTTCG
bamA _F	CCCGTTTCAACATCGACTCT
bamA _R	GGTCACTTTGGTGCCGTTAT

References

1. Jiang, L., Moehle, K., Dhanapal, B., Obrecht, D., and Robinson, J. A. (2000) Combinatorial biomimetic chemistry: Parallel synthesis of a small library of ß-hairpin mimetics based on loop III from human platelet-derived growth factor B. *Helv. Chim. Acta* **83**, 3097-3112
2. Besanceney-Webler, C., Jiang, H., Zheng, T., Feng, L., Soriano del Amo, D., Wang, W., Klivansky, L. M., Marlow, F. L., Liu, Y., and Wu, P. (2011) Increasing the Efficacy of Bioorthogonal Click Reactions for Bioconjugation: A Comparative Study. *Angew. Chem. Int. Ed.* **50**, 8051-8056
3. Güntert, P., Mumenthaler, C., and Wüthrich, K. (1997) Torsion angle dynamics for NMR structure calculation with the new program Dyana. *J. Mol. Biol.* **273**, 283-298

A Peptidomimetic Antibiotic Targets Outer Membrane Proteins and Disrupts Selectively the Outer Membrane in Escherichia coli

Matthias Urfer, Jasmina Bogdanovic, Fabio Lo Monte, Kerstin Moehle, Katja Zerbe, Ulrich Omasits, Christian H. Ahrens, Gabriella Pessi, Leo Eberl and John A. Robinson

J. Biol. Chem. published online December 1, 2015

Access the most updated version of this article at doi: 10.1074/jbc.M115.691725

Alerts:
- When this article is cited
- When a correction for this article is posted

Click here to choose from all of JBC's e-mail alerts

Supplemental material:
http://www.jbc.org/content/suppl/2015/12/01/M115.691725.DC1.html

This article cites 0 references, 0 of which can be accessed free at
http://www.jbc.org/content/early/2015/12/01/jbc.M115.691725.full.html#ref-list-1

Downloaded from http://www.jbc.org/ at UZH Hauptbibliothek / Zentralbibliothek Zuerich on February 8, 2016